PASSIVE MIXING ON MICROFLUIDIC DEVICES VIA DIELECTRIC ELASTOMER ACTUATION

by

KEVIN JEROME MCDANIEL

B.S., TEXAS SOUTHERN UNIVERSITY, 2006

A THESIS

submitted in partial fulfillment of the requirements for the degree

MASTER OF SCIENCE

Department of Chemistry
College of Arts and Sciences

KANSAS STATE UNIVERSITY
Manhattan, Kansas

2008

Approved by:

Major Professor
Dr. Christopher Culbertson

Copyright

Abstract

Mixing is an essential process to many areas of science for example it is important in studying chemical reaction kinetics, chemical synthesis, DNA hybridization and PCR amplification. Mixing on the macroscale level is readily achieved through convection. Rapid mixing on microchips however, is problematic as the low Reynolds numbers and high Péclet numbers indicate that fluid flow is in the laminar regime and limits mixing on microchips to diffusion. Because of these limitations mixing on microchips is often relegated to diffusional mixing which requires long channels and long time periods. Several methods have been developed to increase the speed and efficiency of mixing on microfluidic devices. A variety of techniques have been employed to overcome these obstacles including for example 1) 3 dimensional channel designs to split up and recombine flows 2) employing sophisticated lithographic techniques to make grooves within a channel to generate transverse flows and 3) using lateral flow created by using spiral channels. Other groups have used outside energy sources to achieve mixing by changing of the zeta potential within the channel, using induced charge electroosmosis, and also by modifying the electrokinetic flow. We propose using dielectric elastomers (DEs) to modulate flow as a means to achieve rapid and active mixing on the microchip format. Electroactive polymers such as poly(dimethylsiloxane) function as DEs and are capable of converting electrical energy into mechanical energy. The application of an electrical potential across the PDMS results in a change in the dimensions of the PDMS dielectric layer between the two actuating electrodes creating an actuator. When employed in microfluidic devices this actuator can be used to change the volumes of the microfluidic channels

on the PDMS. If the actuators are placed near a T-intersection where two components are entering the intersection the actuators can serve to improve mixing on microfluidic devices. Studies were conducted on how on the magnitude of the actuation, the frequency of actuation, the field strength, the electrode design and position relative to the T intersection, the channel dimensions and the overall channel design impacted mixing efficiency. Mixing results showed promise but further development of technology is necessary to achieve adequate mixing in microfluidic channels using DEs.

Table of Contents

List of Figures vii
Acknowledgements ix
Dedication x
CHAPTER 1 - Mixing in Microfluidics 1
1.1 Passive Mixing on Microchips 3
1.1.1 Mixing in Planar Spiral Microchannels (1) 3
1.1.2 Mixing in connected-groove channels (2) 6
1.1.3 Split and Recombine Micromixer (3) 8
1.2 Active Mixing on Microchips 9
1.2.1 Zeta-potential Manipulation (4) 10
1.2.2 Induced charge electroosmosis (5) 13
1.2.3 Electrokinetic flow modulation (6) 15
1.3 Conclusion 17
References 19
CHAPTER 2 - Dielectric Elastomers 20
2.1 Energy Conversion in Dielectric Elastomers 20
2.2 Electroactive Polymers as Dielectric Elastomers 21
2.2.1 Piezoceramics/Piezoelectrics 22
2.2.2 Relaxor Ferroelectric Polymers 22
2.2.3 Conducting Polymers 23
2.2.4 Carbon Nanotube Actuators 24
2.3 Physical and Chemical Characteristics of DEs 24
2.4 Performance of Silicon Elastomers 25
References 28
CHAPTER 3 - Electroactive Polymer Mixing on Microchips 29
3.1 Device Rationale 29
3.2 Experimental 30
3.2.1 Chemicals 31

3.2.2 SU-8 Lithography 31
3.2.3 Electrode Plate Fabrication 32
3.2.4 Soft Polymer Lithography (Fluidic Layer) 32
3.2.5 Soft Polymer Lithography (Thin Layer) 32
3.2.6 Device Completion 33
3.2.7 Fluid flow generation and Data analysis 33
3.3 Results and Discussion 34
3.3.1 Electrode-fluidic Layer Designs 34
3.3.2 Actuation Frequency 38
3.3.3 Fluorescence Profiles 39
3.4 Conclusions and Future Directions 46
Appendix A - Additional images 49
Fluorescence Images of flow created by different actuation frequencies 49

List of Figures

Figure 1-1 Illustration of Deans flows that is produced in spiral microchannel (1). 4
Figure 1-2 Color and gray scale images of eight arc spiral channel (1). 5
Figure 1-3 Image of expansion channel and subsequent vortex that is created (1). 6
Figure 1-4 Diagram of Connected Groove Micromixer: a) CGM-1 b) CGM-2 (2) 7
Figure 1-5 Image of splitting of fluid streams into thinner ones leading to complete mixing (3).. 9
Figure 1-6 Illustration of circulation zone in regions around embedded electrodes. This zone is created from the modulating of the zeta potential within the channel. V_d and V_g are the positive and negative applied potential, 1/k represents the EDL thickness. (4) 11
Figure 1-7 Microscope images of fluid flow in channel before turning on electrodes (a) and after turning them on (b). It is shown that mixing occurs immediately. (4) 12
Figure 1-8 Graph showing that mixing occurs at a faster rate when the electrodes are on. The lower the mixing index the more complete mixing has occurred. (4) 13
Figure 1-9 Illustration of flow fields created around conductors of different shapes (5) 14
Figure 1-10 Experimental (a,c) and modeled (b,d) flow fields (5) 14
Figure 1-11 Calculated and measured mixing rates (5) 15
Figure 1-12 Simulated Flurorescence intensity in microchannel, left image employed various channel geometries, right image, using geometry b (6) 16
Figure 1-13 Intensity profile for low frequency (0.07Hz); (a) represents downstream position 500microns (b) reperesents 1.5mm downstream. (6) 17
Figure 2-1 Illsutration of the deformation of the DE when an electric field is applied due to Maxwell Stress 21
Figure 2-2 Depiction of alignment in ferroelectric polymer once a voltage is applied. (a) is molecular orientation before applied field and (b) is molecular orientation after field is applied. 23
Figure 2-3 Comparison of actuation strain obtained by various EAPs. (a) shows strain as a function of potential, (b,c) shows strain as a function of electric field 26

Figure 3-1 Illustration of polymer deformation upon application of an electric field (left) and removal of electric field (right). 30
Figure 3-2 Illustration of electrode-fluidic layer design used to gather all data for this project. The dimensions are discussed in the text. 37
Figure 3-3 Early electrode-fluidic layer designs. Electrodes are depicted in black..... 37
Figure 3-4 Microscope images of channels during different actuation frequency of 10Hz and electric field differences between electrodes of 1500V at 1mm from intersection. Yellow lines represent channel boundaries 39
Figure 3-5 Image of oscillation produced upon actuation. The area in the boxed region shows example of distance over which the average fluorescence profile was taken..... 40
Figure 3-6 Average fluorescence profile at 1, 3, 5 and 7mm downstream from intersection for 1500V difference between electrodes for 10, 20, 30, 40 and 50Hz actuation frequencies.. 41
Figure 3-7 Average fluorescence profile at 1, 3, 5 and 7mm downstream from intersection for 2000V difference between electrodes for actuation frequencies 10, 20, 30, 40 and 50Hz actuation frequency. 43
Figure 3-9 Mixing Indicies of 1500V and 2000V difference in electrode potential at 10, 20 and 30Hz frequencies of actuation. 45
Figure 3-10 Mixing Indices of 1500V and 2000V electrode difference for actuation frequency of 40 and 50Hz and diffusional based mixing..... 46

Acknowledgements

I would like to thank Dr. Culbertson for his advising during this journey towards my degree. Your tutelage and patience towards me was unbelievable and I am very grateful. You have played a major role in molding me into the chemist I am today by allowing me to do research with you as an undergraduate and then allowing me to continue my education as a graduate researcher in your lab. I appreciate your understanding and support of me and my daughter's relationship and allowing me to travel when I got the "long distance daddy" blues. Thank you for everything and I am convinced that the knowledge I obtained during my stay at Kansas State University will aid in me finding a great career to support myself and my family.

I would also like to acknowledge all of my coworkers for your help when I did not know how to use an instrument or how to perform an experiment, thanks. I want to further acknowledge the Department of Chemistry at Kansas State University for everything; the teaching opportunities, seminars and courses that have all strengthened my understanding of chemistry.

Dedication

This thesis is dedicated to my Lord and Savior Jesus Christ because without Him I am nothing and could not have achieved any amount of success. Secondly, to my daughter, Journey, whom I love with all of my heart and is the motivation of all that I do. Also to my family, (Mom, Chris, Kwanita, Alicia, Jennifer, and Mrs. Alexander) for all of your support and love, I am eternally grateful. I could not have made it through graduate school without you all. And lastly but not least, to all of my true friends, I am thankful for the late night motivational conversations, support, and allowing me to vent to you about my frustrations, fears, doubts and dreams.

CHAPTER 1 - Mixing in Microfluidics

Mixing of fluids is vital in many different areas of chemical analysis; processes such as chemical reactions and chemical synthesis require the mixing of two or more chemicals to create a product (5). The mixing efficiency is extremely important because inefficient mixing impacts percent yield of reactions and whether or not the desired products of a reaction are actually produced (5). Mixing using macro scale instrumentation is quite simple to accomplish via convective flows induced for example by stirring or thermal gradients (1). Mixing on the microscale, however, is significantly more difficult to achieve as the large surface to volume ratio effectively suppresses convective flows. The only effective mixing that occurs on the microscale is through molecular diffusion along concentration gradients. To try to improve mixing in the microscale on microfluidic devices, researchers have reported a variety of novel design structures to reduce diffusion lengths or to try to generate convective or chaotic flows using external energy sources as discussed below.

Mixing in macro scale instrumentation is accomplished readily because of the existence of turbulent. It is critical in a variety of systems to either minimize or maximize turbulent flow. As such it is important to be able to predict whether a particular pipe/channel design will generate turbulent flow or not. The ability to predict under what conditions a flowing fluid will generate turbulent flow was first demonstrated by Osborne Reynolds almost 125 years ago. Mr. Reynolds showed that the condition under which turbulence was generated was governed by the value of the ratio of the inertial forces to viscous forces in a given system as the equation below shows:

Equation 1

$$\mathrm{Re} = \frac{Vd}{\nu}$$

where V is the velocity of fluid flow, d is the characteristic length of the channel and ν is the kinematic viscosity. Reynolds number values for turbulent flow are between 2000 and 4000 and below 100 when laminar flow is present (1). It is this low inertial forces in relation to the viscous forces that inhibits mixing in microfluidic devices. Therefore in microfluidics, molecular diffusion is the only source of mixing for molecules initially separated in two separate flow paths in the same channel that is the only significant source of mixing. Consequently, researchers have developed ways to minimize the distance molecules have to travel to enter the opposing flow stream. Another equation that demonstrates the impediment to mixing in microchannels is the Péclet number which is simply the ratio of the rate of advection (e.g. fluid velocity) to the rate of molecular diffusion as shown in the equation below:

Equation 2

$$Pe = \frac{VL}{D_{mol}}$$

where V is the fluid velocity, L is the characteristic length of the microchannel and D_{mol} is the molecular diffusivity. Thus the fluid flow properties embodied by combining the influences of the Reynolds number and the Péclet number show that under typical fluid flow conditions found in microfluidic channels mixing times can be long. Long mixing times negate one of the most appealing aspects of performing chemical analysis on microchips and that is its potential to generate very rapid analyses. Therefore, it is important to look into ways to shorten mixing times. In general there are two ways in which to try to improve mixing. As mixing generally occurs passively through diffusion one can try to shorten the diffusion distances involved as the

diffusion time is a function of the square of the diffusion distance. Alternatively one could develop a method to actively mix the fluid by generating some type of convective flow on the device. These two approaches to mixing – active and passive - have produced rapid and efficient mixing in microchips and have found applications in different types of chemical analyses.

1.1 Passive Mixing on Microchips

Passive mixers are those mixing techniques that exploit various types of flow fields without the use of any type of external electrical or mechanical forces (1). Several types of passive micromixers have been developed that have employed multiple lithography steps, spiral channels, and grooves within the microchannels (2). All of these designs have achieved successful mixing without using any outside forces. As with all mixing designs, the goal was to increase the interfacial contact between two different flow paths in the shortest distance or time possible.

1.1.1 Mixing in Planar Spiral Microchannels (1)

Ugaz et al. took advantage of the ability to produce Dean flows within microfluidic channels to enhance mixing (1). Dean flows are created when fluids flow through curved paths. While traveling through these curved paths, the fluid experiences centrifugal forces that enhance mixing (1). The magnitude of the Dean number can be calculated using the equation:

Equation 3 $$\kappa = \delta^{0.5} \mathrm{Re}$$

where δ is the ratio of the hydrodynamic radius to the flow radius of curvature and Re is the Reynolds number. Dean flows in spiral channels arise from centrifugal forces as previously stated (1). From a mechanistic perspective, as fluids flow down a curved channel, the centrifugal forces pull the fluid on the outer edge towards the midline and also the fluid on the inner edge is

pulled towards the midline. So by the end of the curve there should be a 180° rotation that causes a complete position switch of the fluids in the channel as illustrated in figure 1-1 (1).

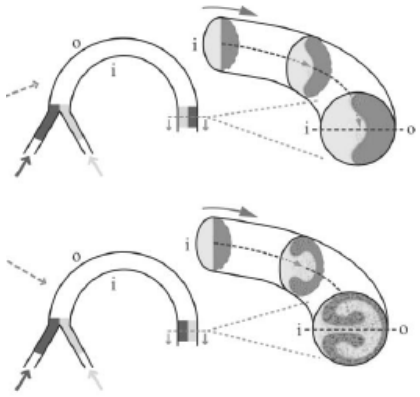

Figure 1-1 Illustration of Deans flows that is produced in spiral microchannel (1).

This group studied fluid mixing in spiral channels that were 150μm wide and 29μm deep. The impact of suddenly expanding the channel width was also studied. This idea of abrupt expansion derived from the idea that a "jet-like" motion is created upon expansion that creates and two vortices that can be used to improve mixing (1). Several channel designs were studied to see which one produced the greatest mixing efficiency. To quantitatively measure the mixing efficiency, the following equation was used:

Equation 4

$$Mixing\,\text{int}ensity = \frac{width\ of\ \ mixed\ \text{int}erface}{width\ of\ \ channel}$$

Furthermore, the flow rate influences the extent of mixing; at higher flow rates efficient mixing occurs quicker than at lower flow rates (1). Ugaz et al. discovered that at higher flow rates 90% mixing can be achieved in 19mm whereas at lower flow rates, 80% mixing occurs within 19mm (1). Moreover, it was found that increasing the length of the spiral contours, almost full mixing could be generated within the first spiral (1). This occurred because of the longer length provided a longer time for diffusion to occur (1). The number of arcs in a spiral was also studied to

determine if this variable had any influence on the mixing time. Spirals containing four, six, eight, and ten arcs were studied and it was shown that the four arc spiral channel achieved 90% mixing by the end of the second spiral and the eight and ten arc spirals achieved 90% mixing by the end of the first spiral (1).

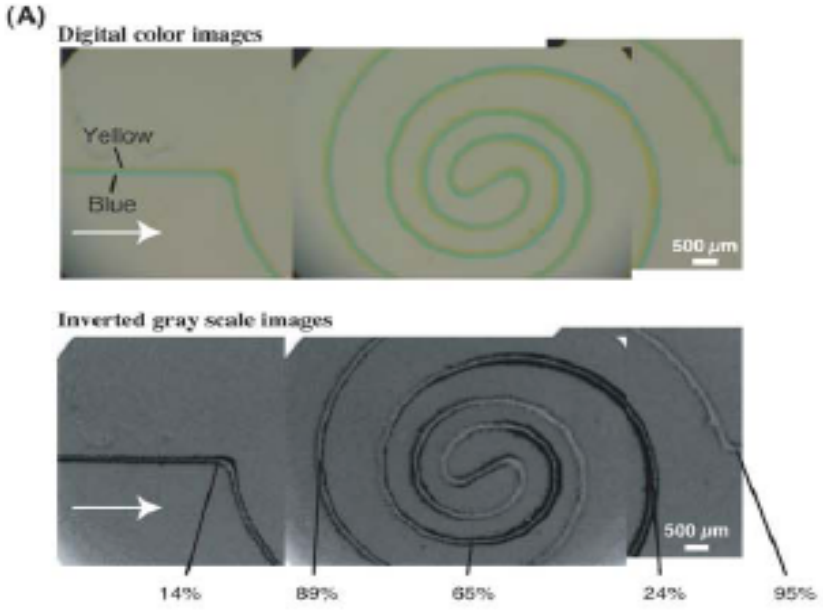

Figure 1-2 Color and gray scale images of eight arc spiral channel (1).

To study the impact of having an expanded section in the channel, a 400μm wide straight section was incorporated instead of the central "S" section while the rest of the channel was maintained at 80μm wide (1). A jet-like motion was produced along with a pair of vortices at the point of expansion. This motion along with the Dean flows resulted in increased mixing. It was found that only at higher flow rates was there a significant increase in mixing (1).

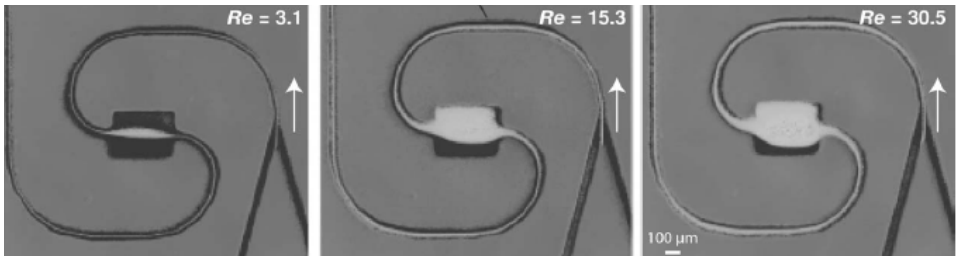

Figure 1-3 Image of expansion channel and subsequent vortex that is created (1).

In conclusion, taking advantage of Dean flows generated in spiral microchannels, aided in achieving passive mixing in short distances. This micromixer required no special laboratory equipment but took advantage of a simple channel fabrication protocol, which was complete in 30 minutes.

1.1.2 Mixing in connected-groove channels (2)

It has been shown that having a large surface to volume ratio provides for greater mass transfer, thus promoting mixing on microfluidic devices (2). Furthermore, chaotic mixing has been created by stretching and folding fluid flows thereby increasing the interface between two fluids and facilitating rapid mixing (2). Many researchers have taken these aforementioned principles and applied them to microfluidic systems to improve mixing efficiencies. The implementation of grooves on the bottom and top of the channel has been shown to improve lateral fluid movement and produced advection within the channel. The resulting mixing happens extremely fast but the fabrication of these micromixers is difficult and time consuming. To circumvent this disadvantage but to take advantage of the mixing efficiency produced by using grooves J. T. Yang et al. have developed a novel fabrication technique to produce a micromixer with grooves (2). Their "connected- groove micromixer" (2) is easy to fabricate using a two step photolithography method. The designs (see figure 1-4) included channels with

slanted grooves on the bottom and sidewalls of the channel, and channels with slanted grooves on the bottom and sidewalls where the grooves on the sidewall were staggered (2). Both sets of grooves were produced at the same time using photolithography (2). To determine the mixing efficiency using the different groove designs several different samples were investigated. Since viscosity has an impact on diffusion and thus mixing, fluids having different viscosities, water/dye solution (low viscosity) and glycerin/water (high viscosity), were used. The relationship between diffusion and viscosity can be obtained using the Stokes-Einstein equation:

Equation 5

$$D = \frac{k_b T}{6\pi\mu R}$$

where k_B is the Boltzmann constant , T is the absolute temperature, R is the radius of solute molecule and μ is the viscosity of the solvent

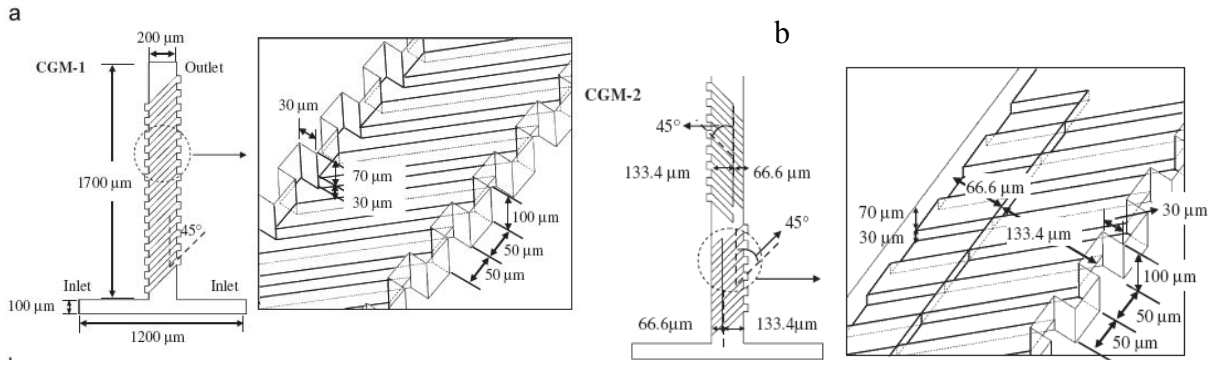

Figure 1-4 Diagram of Connected Groove Micromixer: a) CGM-1 b) CGM-2 (2)

Since solutes in a low viscosity fluid have large diffusivities and solutes in very viscous fluids have little diffusivity, the use of highly viscous fluids will provide a good barometer of the effectiveness of the hypothesized fluid flow produced using the groove-laden channel (2). To determine the applicability of this chip in performing chemical reactions, the mixing of phenolphthalein and sodium hydroxide was investigated. The result of this reaction is a pink

solution and the distance at which this pink solution appears is a good indicator of mixing efficiency of the connected groove micromixer. The efficiency of the micromixer was measured based on the length where the mixing reached 90% (2).

The slanted grooves in channel made the fluids undergo a type of twisting thus increasing the interface between the two flow streams (2). For the slanted, staggered grooves, the flows met at a "saddle" point and a large increase in stretching and folding of the fluids was observed and thus created greater mixing efficiencies (2). Furthermore, for small Reynolds numbers (low velocities) the fluids have enough time for complete diffusion to occur, whereas at mid ranged Reynolds number (Re=1-10, and thus higher velocities) the time that the two fluids streams are in contact with each other is greatly decreased and efficient mixing does not occur at a reasonable time or distance. The mixing indices for the CGM-1 indicate that this design was ~10% more efficient than designs obtained from a basic slanted groove mixer (SGM) for Reynolds numbers between 1 and 100 (2). It was also determined that the mixing index for the CGM-2 design was greater than that of CGM-1 (2). The CGM-2 design also was more than 50% more effective in mixing than the SGM design for Re= 1-100 for a length of 1700μm (2). Further analysis found that the fluids were not mixed completely by the time they arrived at the channel outlet for the CGM-1 and SGM designs whereas for the CGM-2 design, fluids were mixed at distances of less than 12.2mm (2). Overall, mixing efficiencies for both slightly viscous and highly viscous fluids were better using the CGM-2 design.

1.1.3 Split and Recombine Micromixer (3)

Another passive mixing technique that could be implemented onto the microchip format is the "split and recombine" method (3). This method involves three steps to promote mixing: fluid splitting, recombining of the split streams and rearrangement (3). This mode of mixing

could be accomplished using out-of-plane structures to perform the steps necessary for mixing (3). During these steps, the flow streams are split and made "thinner" thereby decreasing the diffusion distance that must be overcome for complete mixing to occur (3). The major drawback to implementing this method seems to be the difficulty in fabricating microfluidic devices with multiple layers of connected channels. Prototypes of this chip have been made but the channel dimensions are outside of the realm that would be considered a microfluidic device with dimensions being 2 mm by 4 mm by 960 mm (width by height by length) (3). From simulations and also from experimental observations on the previously mentioned device, this method of mixing provides efficient mixing at low Reynolds numbers. Figure 1-5 shows the splitting of flow streams into thin lamellae and the eventual mixing observed from optical inspection (2).

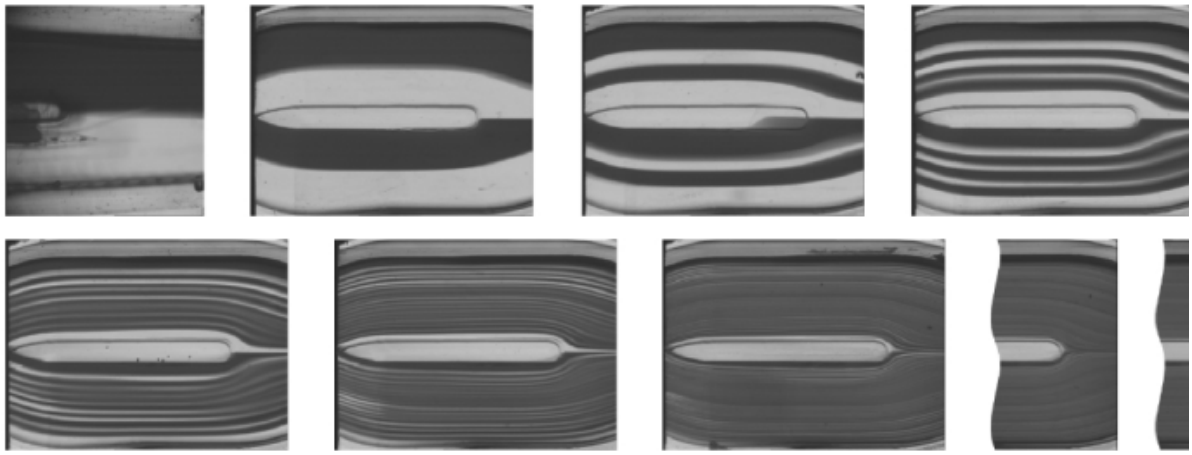

Figure 1-5 Image of splitting of fluid streams into thinner ones leading to complete mixing (3).

1.2 Active Mixing on Microchips

Active mixing involves the use of an external force to produce mixing. Many techniques have been developed by researchers to accomplish satisfactory mixing through the use of zeta-potential manipulation (4), induced charged electroosmosis (5), and the periodic switching of the electroosmotic flow field (5). Unlike many of the passive mixers, the fabrication processes for

these devices are simpler although some of the external hardware necessary to perform mixing is difficult to integrate to the microchip format (4).

1.2.1 Zeta-potential Manipulation (4)

The main method to generate fluid flow on microchips is electroosmosis. Electroosmotic flow (EOF) can be controlled by applying a voltage across the channel or by manipulating the channel wall surface properties (4). The ability to control fluid flow through EOF provides a novel means to mix fluids in microchannels (4). To explain the mechanism for fluid control, an understanding of the zeta potential and its relationship to fluid flow is necessary. To begin with, surfaces of microchannels are generally charged. This charge can be generated in a variety of ways, but for glass microfluidic devices the charge is generated through the ionization of silanol groups on the surface of the channels once they are wetted. This charge can also be modified through a variety of covalent and dynamic coating techniques (4). The charge on the wall attracts counter ions from solution to satisfy the principle of electroneutrality (4). Accumulation of charge in the solution near the channel wall results in an electrical double layer (4). The first part of this electrical double layer consists of counterions that are partially desolvated and that strongly interact with the surface charges on the wall. As all of the charge is not neutralized by this first layer, a second more diffuse layer of counterions forms near the wall surface (4). When an electrical potential is applied to the channel, the ions in the diffuse region move along the channel according to their charge and frictionally drag the bulk fluid with them (4). The velocity of the ions generated by this phenomenon (electroosmosis) can be described using the equation:

Equation 6

$$V_{eo} = -\frac{\varepsilon\varepsilon\zeta}{\eta}E$$

where ε_0 is the permittivity of free space, ε_r is the dielectric constant of the buffer solution, ζ is the zeta potential, η is the viscosity of fluid, and E is the applied electric field. Thus from the above equation, it is evident that the velocity and the direction of the fluid flow is dependent on the zeta potential.

To manipulate the zeta potential of the channel and thus promote mixing in the channel, embedded aluminum electrodes have been employed by the Liu group (4). By varying the potential applied to these electrodes, the charge density can be changed and therefore the zeta potential can be modulated (4). If designed properly varying the zeta potential along the length of the mixing channel leads to a "circulation zone" and thus creates an area of mixing (4). This zone causes the mixed solution to return to the unmixed region upstream from it and promotes mixing (4).

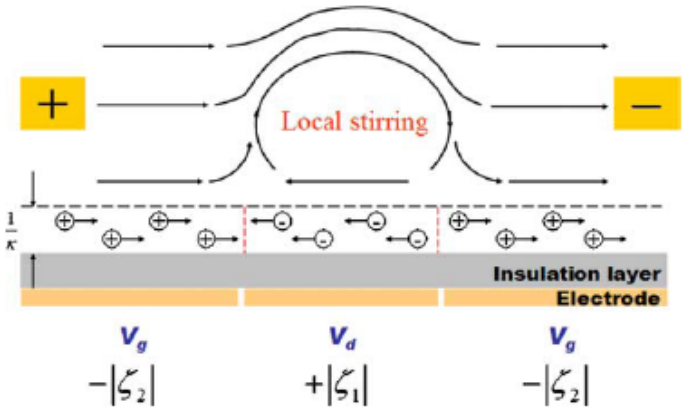

Figure 1-6 Illustration of circulation zone in regions around embedded electrodes. This zone is created from the modulating of the zeta potential within the channel. V_d and V_g are the positive and negative applied potential, 1/k represents the EDL thickness. (4)

Factors such as pH and electrolyte concentration impact the electrical double layer and thus the zeta potential so attention must be paid to these factors (4). It was shown that the lower the pH

and electrolyte concentration, the easier it was to manipulate the zeta potential. Furthermore, it was shown that there was no mixing except that due to diffusion when the embedded electrodes were off (4).

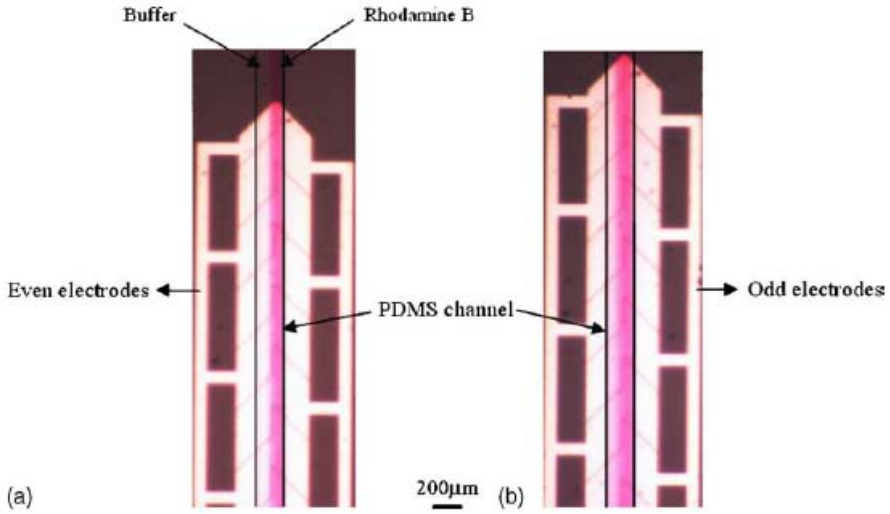

Figure 1-7 Microscope images of fluid flow in channel before turning on electrodes (a) and after turning them on (b). It is shown that mixing occurs immediately. (4)

As soon as the electrodes were activated, mixing was observed. Moreover, 90% mixing was achieved in about 5 mm (4).

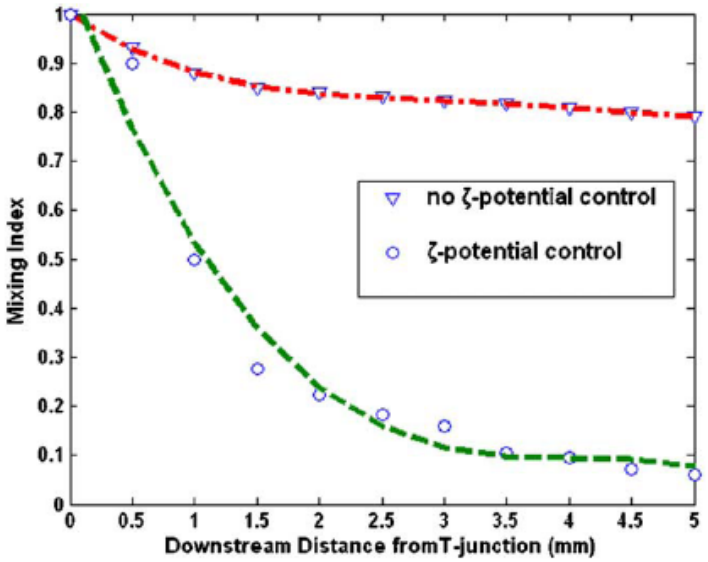

Figure 1-8 Graph showing that mixing occurs at a faster rate when the electrodes are on. The lower the mixing index the more complete mixing has occurred. (4)

1.2.2 Induced charge electroosmosis (5)

Induced charge electroosmosis (ICEO) occurs when a conductor is in a liquid when an electrical potential is applied (5). ICEO generates a variety of flow patterns within the channel around the conductors. The flow pattern is dependent on the field around the conductors which in turn is determined by its shape (5). Therefore, an understanding of the behavior of the conductor is essential to understanding the flow pattern that will facilitate effective mixing. In brief, the conductor is free of current and becomes polarized in an electric field to maintain an internal current of zero (5). Under these conditions, the conductor attracts counter ions from the electrolyte and generates a type of electrical double layer (5). The mobile ions in solution move in response to the field and drag the surrounding fluid. The pattern of the flow around the conductor is determined by the shape of the conductor (5). Symmetric conductors, such as cylinders produce four symmetric vortices and asymmetric conductors, such as triangular conductors, produce non- symmetric flow patterns.

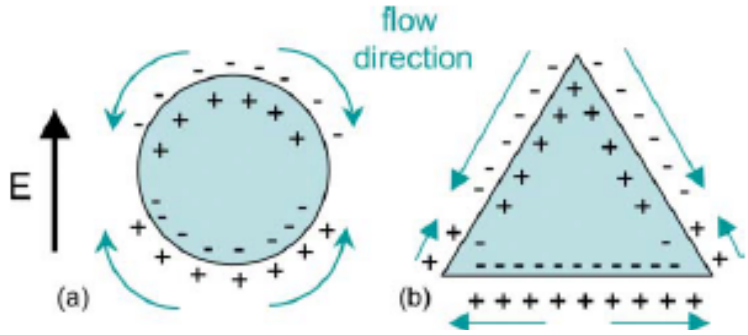

Figure 1-9 Illustration of flow fields created around conductors of different shapes (5)

Results showed that when using cylindrical shaped conductors, symmetric flows that do not mix at an appreciable distance from the conductor and do not produce sufficient mixing (5). Therefore, a triangular shape conductor was implemented. When an electrical field was applied, a mixing zone was created and fluid transport occurred from the base to the tip of the triangle, thus mixing the fluids located at the top and bottom of the channel (5). When quantitatively measured, 63% mixing was achieved in 6.4 seconds (5).

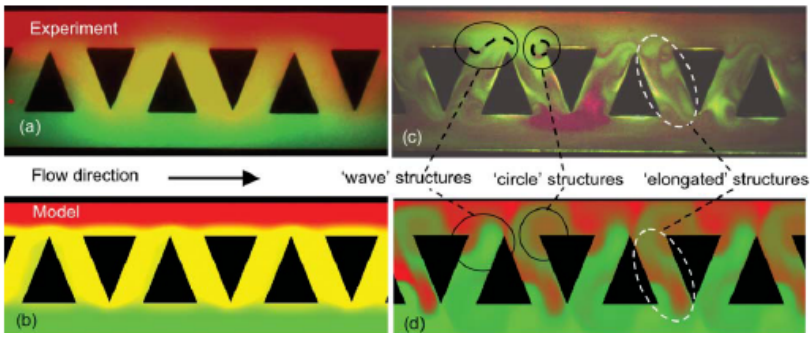

Figure 1-10 Experimental (a,c) and modeled (b,d) flow fields (5)

At higher applied voltages, mixing occurred in less than a second. Furthermore, the model predicted a mixing rate that was 4 times faster that observed during experimentation.

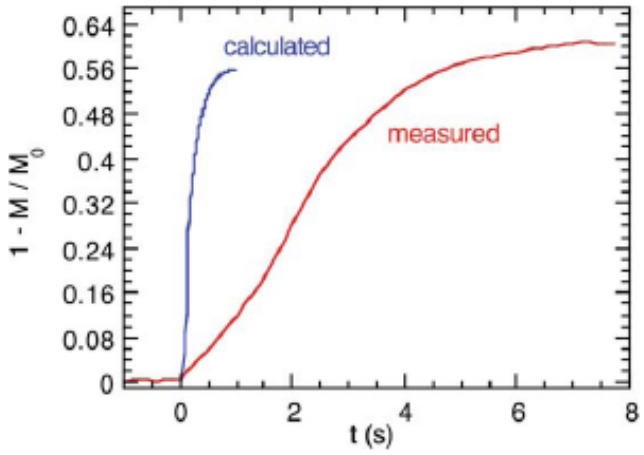

Figure 1-11 Calculated and measured mixing rates (5)

1.2.3 Electrokinetic flow modulation (6)

Injection of analytes in varying concentrations on microchips is important and has applications in biomedical sciences and material processing. Injection can be accomplished through the modulation of the potential in one of the fluid reservoirs on the microchip (6). When two flow streams of different compositions are moved through a microchannel laminar flow occurs. When the potential applied in one reservoir is floated a type of banded injection occurs but the band spans the entire width of the channel thereby mixing the two flow streams. This idea was confirmed both using simulations and experimentation.

Through mathematical derivations two important factors contribute to the mixing of the two flow streams: the Peclet number and a dimensionless frequency (6). This dimensionless frequency term can be calculated from the equation:

Equation 7

$$f^* = f\frac{W}{U}$$

where f is the switch frequency, W is the width of the channel and U is the average velocity. It was shown that for large Peclet numbers convection dominates and for Peclet numbers much less than 1, diffusion will dominate the system (6). Furthermore, it was shown that mixing occurred

for smaller f* (6). To accomplish complete mixing, the fluid from one of the diverging channels must span the width of the channel and it was shown that this only occurs at lower f' values and high velocities see figure 1-12 (6). Moreover, the fluorescent profiles for the higher frequencies indicated that the mixing only spanned half of the channel width, figure 1-6. From this data it was concluded that two different types of flow can be generated both dependent upon frequency. In addition it was concluded that the extent of mixing increased as electric field increased (6). Overall mixing was accomplished using this electric field modulation. This method is similar to the method we will use except that modulation will be induced by pressure differentials and electric field modulation.

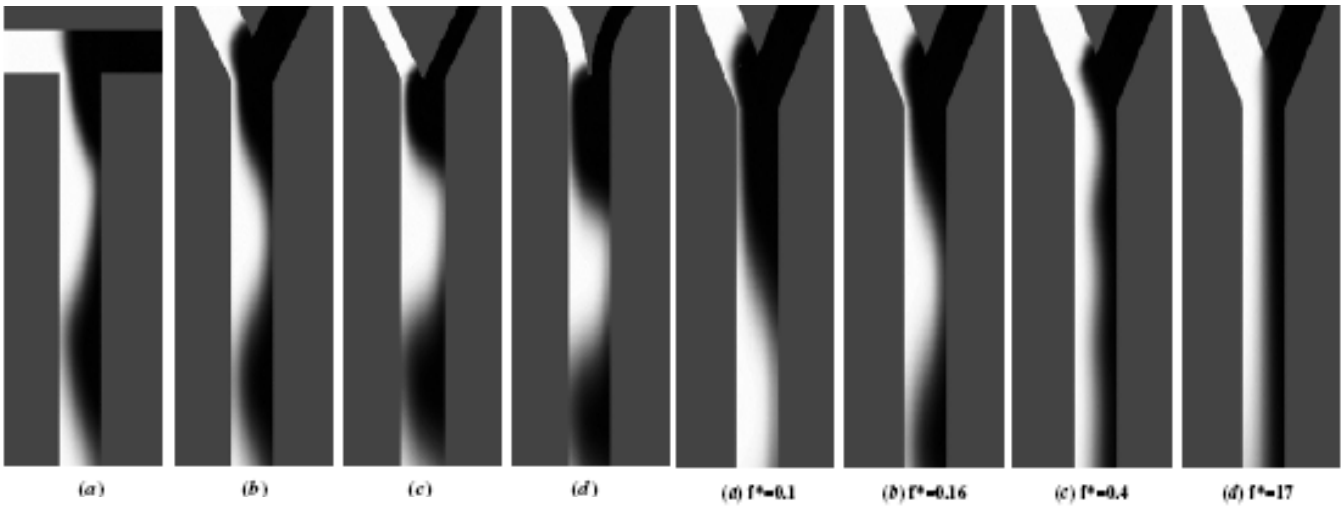

Figure 1-12 Simulated Flurorescence intensity in microchannel, left image employed various channel geometries, right image, using geometry b (6)

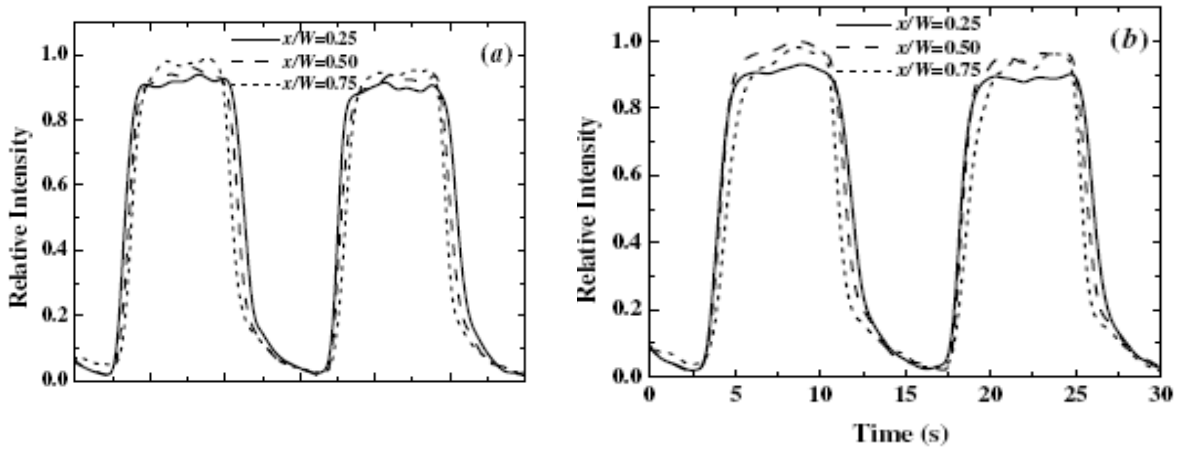

Figure 1-13 Intensity profile for low frequency (0.07Hz); (a) represents downstream position 500microns (b) reperesents 1.5mm downstream. (6)

1.3 Conclusion

Mixing can be accomplished through a variety of means that range from modifying the channel geometry and taking advantage of Dean flow (1), fabricating structures, such as grooves, within the channel itself, and by having multiple layers of fluid flow and therefore being able to split flow streams into smaller, thinner ones and facilitating faster mixing. All of the methods fall under the umbrella of passive mixing and produce results that can be applied to perform chemical reactions, and study reaction kinetics. Moreover, active mixers have been produced that require an outside force to achieve fluid mixing. These mixers include taking advantage of channel wall chemistry and manipulating the zeta potential (4), using embedded electrodes and causing traverse fluid flows (5), and lastly by modulating the potential of a fluid reservoir to get a banded flow that produces mixing at low modulation frequencies. The methods described above have both drawbacks and advantages that will determine which method best fits the needs of the researcher. Furthermore, there is a need for additional mixing methods, both passive and

active, that can provide highly efficient mixing in shorter distances or times. These mixers will be beneficial in many areas of chemistry and biomedical sciences

References

1. Arjun P. Sudarsan, Victor M. Ugaz, *Lab on a Chip,* 2006,3, 74
2. Jing-Tang Yang, Wei-Feng Fang, Kai-Yang Tung, *Chemical Engineering Science*, 2008, 63, 1871
3. F. Schonfeld, V. Hessel, C. Hofmann, *Lab on a Chip, 2004, 4, 65*
4. Hsin-Yu Wu, Cheng-Hsien Liu, *Sensors and Actuators A: Physical,* 2005, 118, 107
5. Cindy K. Harnett, Jeremy Templeton, Katherine A. Dunphy-Guzman, Yehya M. Senousy, Michael P. Kanouff, *Lab on a Chip*, 2008, 8, 565
6. Zhongliang Tang, Seungbae Hong, Djordje Djukic, Vijay Modi, Alan C. West, James Yardley, Richard M. Osgood, *Journal of Micromechanics and Microengineering*, 2002, 12, 870
7. Chih-Chang Chang, Ruey-Jen Yang, *Microfluid NanoFluid*, 2007, 3, 501

CHAPTER 2 - Dielectric Elastomers

Dielectric elastomers (DE) are transducers that convert energy of one form to another (7). They are normally classified into two categories: generators or actuators. Generators are devices that can convert mechanical energy to electrical energy and actuators are devices that can convert electrical energy into mechanical energy (7). The typical design of a DE is composed of a thin polymer film sandwiched between two electrodes (7). This design is analogous to that of a capacitor in which a dielectric component is between two conductors and energy storage is achieved. In this chapter, the important parameters of DEs that allow them to be used actuators will be briefly explained. These parameters include 1) the energy conversion mechanism and its impact on the DE 2) a comparison of several electroactive polymers that function as DEs 3) the physical and chemical characteristics of DEs, and 4) a discussion of the advances that have been made in using DEs as actuators.

2.1 Energy Conversion in Dielectric Elastomers

Dielectric elastomeric actuators convert applied electrical potentials into mechanical energy (7). The amount of energy that is generated during actuation can be determined starting from the assumption that the total volume of the elastomer remains the same upon actuation. To generate actuation an electric potential is applied across the dielectric through the electrodes. This results in the accumulation of opposite charges on each side of the dielectric. It is these two phenomena that convert the applied electrical potential to mechanical energy which is evident by the deformation of the thin film polymer as can be seen in figure 2-1.

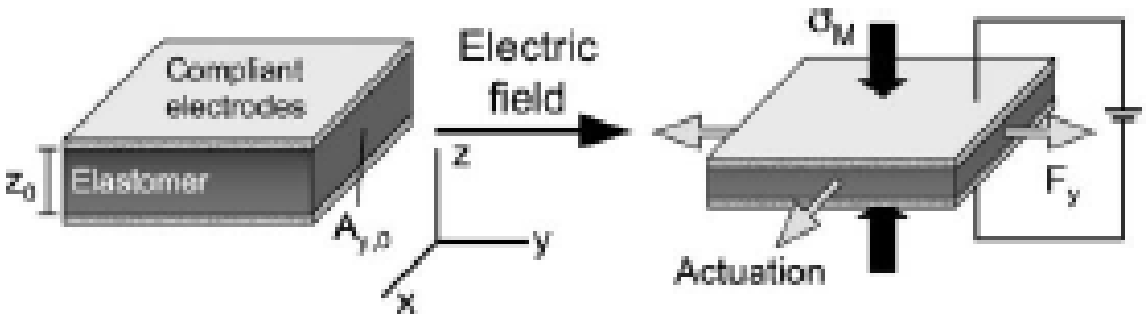

Figure 2-1 Illsutration of the deformation of the DE when an electric field is applied due to Maxwell Stress

Therefore, the DE film should decrease in one direction and increase in another upon the application of an electric field across the dielectric if the electrodes themselves are free to move. The motion that is produced by these forces is known as the Maxwell stress and is given by the equation:

Equation 8 $$P = \varepsilon\varepsilon_0 E^2$$

where E is the electric field strength, ε is the dielectric constant and ε_0 is the permittivity of free space. It is evident from the equation that the amount of displacement of the polymer is directly proportional to the dielectric strength of the polymer and the magnitude of the applied electric field.

2.2 Electroactive Polymers as Dielectric Elastomers

It is important to be able develop actuator technology that not only delivers a lot of power per unit volume but also that does it efficiently and fast (7). Several materials have been investigated for use as dielectrrics in dielectric actuators and the results generated have shown extraordinary promise for several of these dielectrics to be used in actuators. Some even have properties that rival and mimic the properties of natural muscle. This has led to some DEs to be

referred to as artificial muscle (7). Other potential interests in DEs include generating more sophisticated alternatives to combustions engines alternatives that possess the ability to make precise movements without using too much energy but that have the same power density output (7). Several different actuator materials will be discussed and the advantages and disadvantages that are characteristic to each one.

2.2.1 Piezoceramics/Piezoelectrics

In piezoceramics, an electric field acts on dipoles found in the material. This leads to deformations in the crystalline domains and causes strain (7). This strain can be used to change the shape of the material over very short distances as a function of the amount of strain. The strain induced is directly dependent on the magnitude of the applied voltage and changes in strain are limited to only about 0.1% (7). Another fascinating characteristic of piezoceramics is that if a constant voltage is applied a constant position is maintained (7). Piezoelectrics are used in small distance applications including subatomic positioning. Larger positioning distances can be obtained by stepping up the applied voltage (7).

2.2.2 Relaxor Ferroelectric Polymers

Electrostrictive polymers are another class of polymers that have the ability to convert electrical energy into mechanical motion (7). This class of polymers includes ferroelectric polymers, liquid crystals and graft elastomers (7). Ferroelectric polymers change conformation due to electrostatic forces (7). When an electric field is applied the polar functional groups align with the field causing the molecular groups that are perpendicular to field to in length, figure 2-2 (7). Furthermore, these polymers are stiff thus the amount of strain induced is small (7). This small strain is due to the stiffness and that some of the electrical energy goes to the actual deformation of the polymer (7). Strain values of only 3-10% have been achieved using these

materials, however high work densities have been achieved that surpass those obtained using DEs (7).

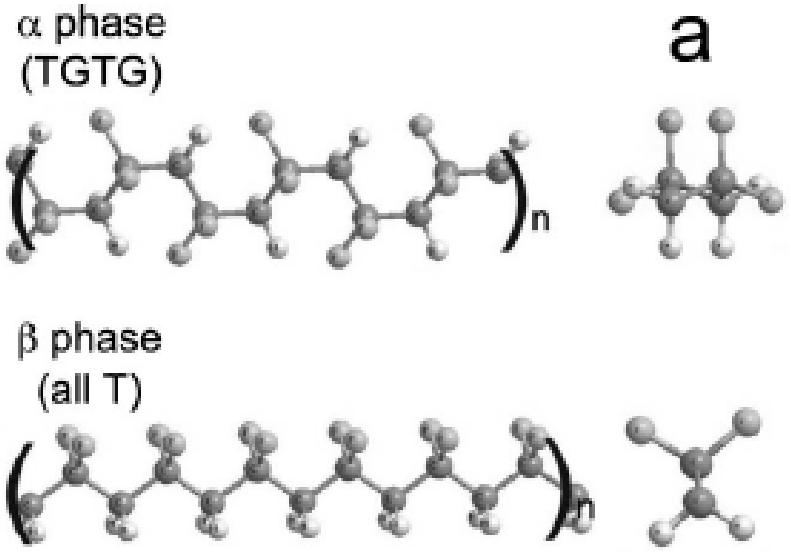

Figure 2-2 Depiction of alignment in ferroelectric polymer once a voltage is applied. (a) is molecular orientation before applied field and (b) is molecular orientation after field is applied.

2.2.3 Conducting Polymers

The need to use high voltage for operation causes problems in experimental designs due the requirement for additional electronics, and the possibility of additional packaging (7). Thus the need for materials that can be operated at lower applied voltages is necessary. This desired characteristic led to the use of conducting polymers as sources of actuators. When a potential is applied to a conducting polymer through an electrolyte, electrons are added or removed from the polymer (7). When ions are added to the polymer, swelling occurs perpendicular to the chain shown to be proportional to the number of ions that penetrate the polymer. Strain values of about 8% have been achieved which is much lower than those obtained us DEs (7).

2.2.4 Carbon Nanotube Actuators

Low strains values between 0.1 and 0.6% have been achieved using carbon nanotubes. When immersed in an electrolyte solution and an electrical potential is applied the charges are attracted to the solution/tube interface (7). This results in changes in electrostatic forces and changes in electron density, thereby, producing changing in length. These length changes are much less than those obtained using DEs (7).

2.3 Physical and Chemical Characteristics of DEs

An elastomer is a macromolecular material that changes when exposed to mechanical loads (7). They are usually made by crosslinking a polymer by through the use of a chemical initiator or radiation. Elastomers are classified into three different groups- chemically crosslinked rubbers, physically crosslinked thermoplastic elastomers, and entangled polymers of high chain length. Poly(dimethylsiloxane) (PDMS) is a polymer that is used very often and functions as a DE. PDMS has a low dielectric constant, high dielectric breakdown strength and high chain mobility. The dielectric constant is low because of the lack of polar groups present. Polyurethanes are also often used as DEs and have a dielectric constant between 3 and 10 (7). They suffer from low dielectric strength because of their higher ionic conductivity (7).

Elastomers have both liquid and solid attributes. Their elastic attributes are derived from the cross linking process and the viscous attributes come from the presence of long polymer chains (7). The elasticity of a polymer is determined by its Young's modulus (Y) or the elastic modulus (G). The elastic properties of an elastomer functioning as an actuator are important because they determine the maximum Maxwell stress that occurs when voltage is applied.

Furthermore, the softer or more elastic the polymer the less voltage that has to be applied to obtain the desired polymer displacement.

2.4 Performance of Silicon Elastomers

The performance of silicone DEs is determined by several factors and dictates what polymer is best for the chosen task. DEs performance is based on the interaction between charges on opposite sides of the polymer film (7). The strain that occurs when an electrical potential is applied is given by the equation:

Equation 9

$$S_z = \frac{\varepsilon_0 \varepsilon E^2}{Y}$$

where ε is the dielectric constant, E is the applied electric field, Y is the Young's modulus, and ε_0 is the permittivity of free space. This equation shows that the performance of the polymer is based on innate characteristics of the polymer; the dielectric constant, and Young's modulus (7). Furthermore, the magnitude of the applied voltage will increase the strain experienced by the polymer. Another important factor that must be considered when using DEs is their characteristic energy density (7). It is desirable to be able to store as much energy as possible per unit volume. Moreover, high electrical breakdown is also an important so the largest response is achieved. In general there are six features that are important to optimize the response: (1) high bulk resistance and low electrical loss, (2) low viscoelastic damping, (3) good electrical fatigue properties, (4) good mechanical fatigue properties, (5) temperature tolerance and (6) ease in manufacturing of thin films (7).

Silicones and acrylic elastomers have received the most attention from researchers and also have exhibited the best performance. One finding that has contributed to their great performance is the introduction of pre-strain (7). This is accomplished by stretching and holding the film in tension before measurements are made (7). It has been shown that the maximum

strain and pressures experienced are greatly increased by implementing pre-strain. Furthermore, researchers have used different silicone fluids and hardeners to determine what impact hardener concentration had on the strain produced (11). It was found that increasing the hardener concentration by 5% increase the Young's modulus by 40% (11). By increasing the Young's modulus the breakdown field was also increased (11). The dielectric constant can also be tuned by combining different types of or by blending in a copper phthalocyanine oligomer (11). With the addition of this oligomer the silicone based elastomer's dielectric constant was increased from 3.3 to 11.8 (11). Overall, silicone elastomers show higher actuation strains that all other classes of electroactive polymers (EAPs) save those acrylate based polymers. Figure 2-3 shows the percent strains of various EAPs and it shows the superior performance of silicones over the other polymers.

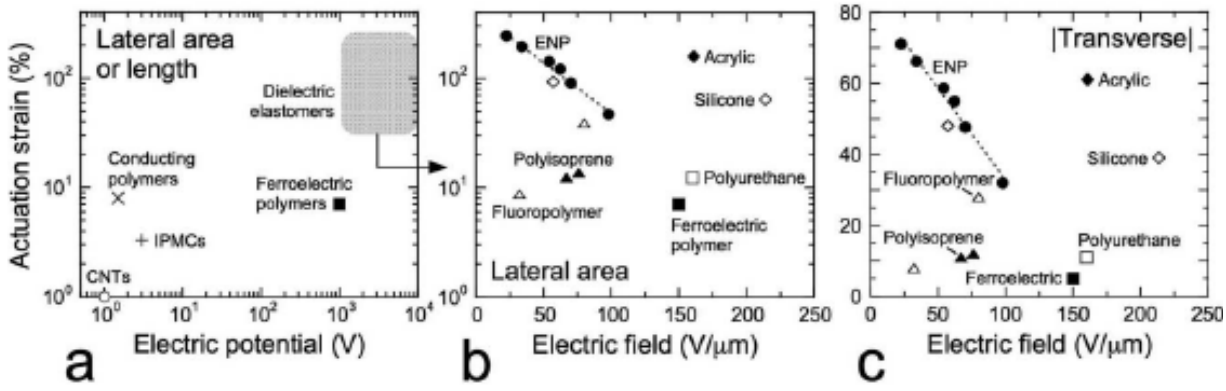

Figure 2-3 Comparison of actuation strain obtained by various EAPs. (a) shows strain as a function of potential, (b,c) shows strain as a function of electric field

Through the use of the pre-strain technique, silicone strains of 117% were achieved (11). This is significantly less than the 215% that was achieved by the acrylic elastomers but the acrylic suffers from buckling due to the pre-strain tension being released (11). Furthermore, efficiencies of 80-90% are theoretically obtainable because of the less loss of viscoelasticity, and low

electrical leakage. In general, silicones are superior to acrylics, in the fact that the dielectric loss factor and mechanical loss factors at high frequencies are much lower in silicones. Finally, the overall maximum efficiency is higher at high frequency actuation for silicones than in acrylics. From an environmental condition standpoint, silicones are also superior to acrylics because they exhibit constant mechanical properties aver temperature ranges of -65°C -240°C and as far as -100C for one silicone rubber (7). Acrylic elastomers only have temperature ranges of about -10°C - 80°C (7). In conclusion, silicones exhibit many attractive features that make them a desirable material for actuator technology using electroactive polymers.

References

1. Chang Liu, *Advanced Materials*, 2007, 19, 383
2. Roy Kornbluh, Ron Pelrine, Harsha Prahlad, Richard Heydt, *MEM/MOEMS Components and their applications*, 2004, 5344, 13
3. N. Galler, H. Ditlbacher,, B. Steinberger, A. Hohenau, M. Dansachmuller, F. Camacho-Gonzales, S. Bauer, J.R. Krenn, A. Leitner, F.R. Aussenegg, *Applied Physics B*, 2006, 85, 7
4. Ronald E. Pelrine, Roy D. Kornbluh, Jose P. Joseph, *Sensors and Actuators A*, 1998, 6, 77
5. I. Krakovsky, T. Romjin, A. Posthuma de Boer, *Journal of Applied Physics*, 1999, 85, 628
6. Ravi Shankar, Tushar Ghosh, Richard Spontak, *Soft Matter*, 2007, 3, 1116

CHAPTER 3 - Electroactive Polymer Mixing on Microchips

Since mixing on microchips has proven to be difficult using both active and passive methods new technologies are necessary to overcome the obstacles that impede rapid and efficient mixing on microchips. Active mixing methods suffer from the necessity of bulky external equipment to provide energy to drive the mixing process and passive mixing methods suffer from complex device fabrication. To overcome these obstacles a novel device that is simple to fabricate and takes advantage of the actuation ability of dielectric elastomers (DEs) has been developed. This mixing method shows incredible promise as an additional means to achieve rapid and efficient mixing. Several parameters were studied; channel design, electrode design including shape and size, frequency of actuation, and field strength. The mixing efficiency was based on the fluorescence profile taken across the width of channel at different points downstream. A flat fluorescent profile across the entire width of the channel was taken to be indicative of complete mixing. The distance downstream where complete mixing occurred was compared to the distance downstream where complete mixing occurred solely based on diffusion. Although, initial device designs showed no drastic improvement over diffusion-based mixing, there are several modifications that can be made that should be able to improve the mixing results. Issues such as using hydrodynamic flow, going to more extreme actuation frequencies, modifying channel designs and using different elastomers all could solve the shortcomings of the prototype. The reasons for these suggested modifications will be addressed along with results from the initial device.

3.1 Device Rationale

Poly(dimethylsiloxane) (PDMS) is at the most popular elastomeric material used to fabricate microfluidic devices. It has several desirable characteristics that make it the material of choice for microfluidic based studies. One of the characteristics of PDMS that has recently gotten a lot of attention is its ability to function as a dielectric elastomer. This property allows PDMS to convert electrical energy into mechanical energy. It is this ability that was exploited to achieve mixing on microfluidic devices. From a mechanistic perspective, the change in the polymer's shape induced by the electric field produces a "crater" where additional fluid volume rushes into until the potential is released. Once the potential is released and the polymer relaxes back to its original state, the fluid that was in the "crater" is expelled and pushed into the other fluid flow stream. It is this actuation of the polymer that increases the interface between the two fluid flow streams. The decrease in the fluid interface allows diffusion to occur more rapidly thus achieving mixing in shorter times or distances downstream. The advantages of this device include the simple fabrication protocol that relied on well-developed lithography techniques, the requirement of only a power supply that could be replaced by batteries for field testing, and the robust nature of the device.

Figure 3-1 Illustration of polymer deformation upon application of an electric field (left) and removal of electric field (right).

3.2 Experimental

3.2.1 Chemicals

Ceric sulfate, sodium borate and potassium hydroxide were all purchased from Fisher Scientific (Pittsburgh, PA). Sodium dodecyl sulfate was purchased from Sigma Aldrach (St. Louis, MO). 2,7 Dichlorofluorescein was purchased from Acros Organics (Morris Plains, NJ). Sylgard 184 silicon elastomer kits used for making PDMS were purchased from Dow Corning (Midland, MI). All chemicals were used as received.

3.2.2 SU-8 Lithography

A clean, 4 inch silicon wafer (Silicon Inc., Boise, ID) was coated with 4ml of SU-8 2010 (Microchem, Newton, MA) and spun at a rate that produced the desired photoresist thickness of ~20μm. The wafer was then removed from the spin coater and placed on a hotplate set at 95°C for 4 minutes (soft bake). After baking, the wafer was allowed to cool for 3 minutes. Next, the photomask (Fineline Imaging, Colarado Springs, CO) with the desired channel design is placed on top of photoresist coated silicon wafer. To ensure that the mask was flat a quartz plate was laid on top of it. The wafer was then exposed to UV radiation at ~ 50mW/cm^2 from a UV flood exposure system (Oriel Instruments, Stratford, CT) for 4s. After exposure, the wafer was then placed on a 95°C hotplate for 4 minutes (hard bake). Next, the wafer was placed in the developing solution, propylene glycol monomethyl ether acetate (Aldrich, Saint Louis, MO), for 3-4 minutes. The developed wafer was then immediately rinsed with isopropanol and dried under a nitrogen stream. The height of the SU-8 features were then measured using and XP-2 profilometer from Ambios Technologies (Santa Cruz, CA). The height of the structures corresponds to the channel depth of the PDMS channels.

3.2.3 Electrode Plate Fabrication

5x5x 0.02 inch crown glass plates (Telic Co, Velencia, CA) coated with chrome at a thickness of 1000Å followed by AZ 1500 photoresist at a thickness of 5300Å were used to fabricate electrode plates. To begin, a photomask (Fineline Imaging, Colorado Springs, CO) was placed on top of the plate and made flat by using a quartz plate. Next, the plate was exposed to UV radiation at ~ 50mW/cm^2 for 4s using a UV flood exposure system (Oriel Instruments, Stratford, CT). After exposure the plate was placed in a KOH developing solution for 90 seconds, rotating the plate 90° every 15s. After developing, the plate was thoroughly rinsed with water and placed in a ceric sulfate solution to etch away the unprotected chrome. The plate was rotated 90° every 30 seconds while in the etching solution. After etching away the chrome, the plate was once again rinsed with copious amounts of water. The plate was then cut into two 2x3 inch electrode plates using a dicing saw (Sherline model 5410, Vista, CA).

3.2.4 Soft Polymer Lithography (Fluidic Layer)

To make the fluidic layer where fluid mixing will take place soft polymer lithography was used. First, a 10:1 mixture of Sylgard 184 Elastomer Base (Dow Corning, Midland, MI) to curing agent is thoroughly mixed and degassed. Subsequently, the elastomer mixture was poured onto the silicon wafer containing the channel design and cured for 14 minutes at 80°C. The fluidic layer was then removed from the oven and gently peeled away from the silicon wafer and the channel design is transferred to the elastomer.

3.2.5 Soft Polymer Lithography (Thin Layer)

A mixture of 20:1 Sylgard 184 Elastomer base to curing agent was mixed and degassed. After removal from the dessicator, the PDMS was poured onto the electrode plate (coated with hexamethyldisilazane to prevent the thin layer from permanently adhering to electrode plate) and

spun at 2000rpm for 45 seconds. The subsequent PDMS layer was ~38μm. The electrode plate was then cured at 80°C for 6 minutes.

3.2.6 Device Completion

To complete the mixing device, the electrode plate with the cured thin layer of PDMS was placed under a microscope for alignment. The fluidic layer was then placed in laid down on top of the electrode plate and all air bubbles were removed to make sure a tight seal between the two PDMS layers was achieved. The device was then placed in an 80°C oven for another 50 minutes for further curing. After removing the device from the oven, the excess PDMS is trimmed away from the electrode plate using a razor blade. Next, holes were punched at the channel entrances using a biopsy punch. Glass reservoirs were then attached at the entrances to contain the fluids used for mixing. The reservoirs were cured for 30 minutes. Then, the PDMS layers around the electrodes were cut away using a scalpel. After removing the PDMS around the electrodes, the metal wire was glued on the plate using JB Weld to provide a means of applying voltages and cured at 80°C for ~45 minutes. Lastly, colloidal silver, was used to make an electrical connection between the metal wire and electrode pad and placed in the 80°C oven for 10mins.

3.2.7 Fluid flow generation and Data analysis

Fluid flow was generated by first filling each reservoir with 5mM sodium borate, 1.5mM SDS buffer and pulling on each reservoir with a vacuum for 5 minutes to fill the channels with buffer. SDS was added to the buffer to improve the wettablity of the microchannels. To generate flow via an applied electric field, Pt wires were inserted into the two horizontal channel reservoirs; one containing buffer and the other containing fluoroscein dissolved in buffer to a

concentration of 60μM for microscopy experiments. A third Pt wire was inserted into the waste reservoir at the end of the mixing channel and held at ground. Voltages are then applied through an in-house developed LabView program. For all experiments, field strengths of 500V/cm was used to generate flow. To collect fluorescent profiles, images were taken with a CCD camera at different point downstream while mixing occurred. The fluorescent images were converted into text files and imported into an in-house developed LabView program. The program allowed placement of cursors at different points on the image that designated the region where an average fluorescent profile would be taken. The subsequent files were then uploaded into Igor Data Analysis software where the standard deviation and average fluorescence intensity of the plots were calculated. These values were then used to determine the extent of mixing using our device.

3.3 Results and Discussion

3.3.1 Electrode-fluidic Layer Designs

The goal of this experiment was to try to decrease the diffusion distance between the two streams in order to improve the speed of mixing. The push and pull of the liquid into and out of the intersection should produce vertical bands of samples from the two channels accessory channels into the mixing channel (Figure 3.1). If the vertical band distance is shorter than ½ the channel width then mixing should be improved.

In order to optimize the mixing capabilities, the placement of the electrode in relation to the fluidic layer used to supply the electrical energy needed for actuation is very important. The size of the electrode also plays an important role in how effective the mixing will be. To initially study the effect of electrode placement 2 electrode designs were investigated (Figure 3-1). For both of these electrode designs the same channel structure (i.e. fluidic layer) was used. The

fluidic layer consisted of a Y-channel manifold. The channels that made up the two arms of the Y were 1.4cm long and 130μm wide. The channel that served as the trunk of the Y and the mixing channel was 2cm long and 150μm. All of the channels were 20 μm deep. Electrode Design A (fig 3-1A) consisted of 2 electrodes in the main mixing channel that were 2 cm long and 100 μm wide. Mixing was attempted by applying an electric field between the channel and the electrodes of 500 V/cm. The electrodes were energized 180˚ out of phase with one another at frequencies ranging from 10 to 50 Hz. No mixing or evidence of fluid perturbation during application of the electric field thus this design. Either the electrodes were not large enough to induce a significant volume change in the channel or the fluid motion achieved by the actuators was in parallel with the fluid flow and so did not increase mixing. This design was not investigated any further. Electrode design B consisted of two 300μm wide electrodes positioned near the base of each Y -channel. Design B showed little change to the paths of the individual flow streams. There was evidence of a change in fluid motion but not enough to indicate this design would induce rapid and efficient mixing. To improve the extent of fluid motion, a second generation design was made, figure 3-1C. This design included two 1.2mm wide oval electrodes that could be aligned within the arms of the channel as in design C. In addition, the channel areas directly above the electrodes was expanded a bubble to increase the actuation area ($39mm^2$ versus $156mm^2$), and therefore, allow a greater amount of fluid to be displaced. Figure 3-1 A-C shows the entire complement of electrode-fluidic layer designs used in "Y" mixing. We used the following equation to determine the change in height of the polymer upon actuation and combined this value with the channel dimensions to determine the amount of fluid that would be drawn into the additional polymer volume created by actuation:

Equation 10

$$\frac{\Delta h}{h} = -\frac{1}{2Y}\varepsilon_0 k E^2 (1+2\upsilon)$$

where Δh is the change in polymer thickness upon actuation, h is the initial polymer height, Y is the Young's Modulus of polymer, ε_0 is the permittivity of free space, E is the electric field and ν is the Poisson ratio (0.5 for polymers). For PDMS 10:1 ratio the Δh value was 16.8 microns at a field strength of 500 V/cm thus giving a volume of 0.008 μL that would rush into the additional volume created by actuation of the device with a larger active area. This value would increase at higher field strengths as shown in equation 8. To apply these higher voltages, modifications in channel designs and electrode designs would be necessary. Electrode design C suffered from two flaws: the inability to realign fluidic layer if a hole developed in the chrome electrode would occur due to PDMS breakdown and 2) if too high of a potential was applied and also "cross talk" between the electrodes while in out-of –phase states thereby creating holes in the electrode. To combat both of these issues, a new electrode design was implemented, figure 3-2. This electrode design was implemented and used for all of the results subsequently discussed. The fluidic layer that was paired with this electrode design included a "T" channel design. This design incorporated 1cm long, 100μm wide horizontal arms that had a 400μm expansion halfway to the intersection for an active area of, figure 3-2. At the intersection, the channel width decreased from 100μm to 50μm and then widened back out to 100μm. This constriction was incorporated into the design to decrease the distance for diffusion to occur for mixing. The electrode design also improved on the hole burning issue mentioned previously, more than fifty 30 second mixing experiments at 500V/cm were run before any electrode hole formation was seen.

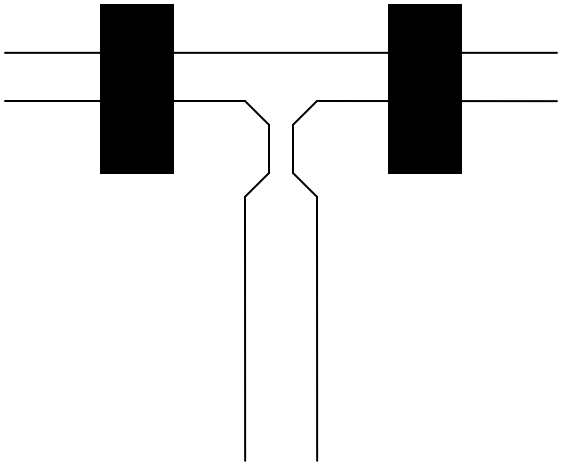

Figure 3-2 Illustration of electrode-fluidic layer design used to gather all data for this project. The dimensions are discussed in the text.

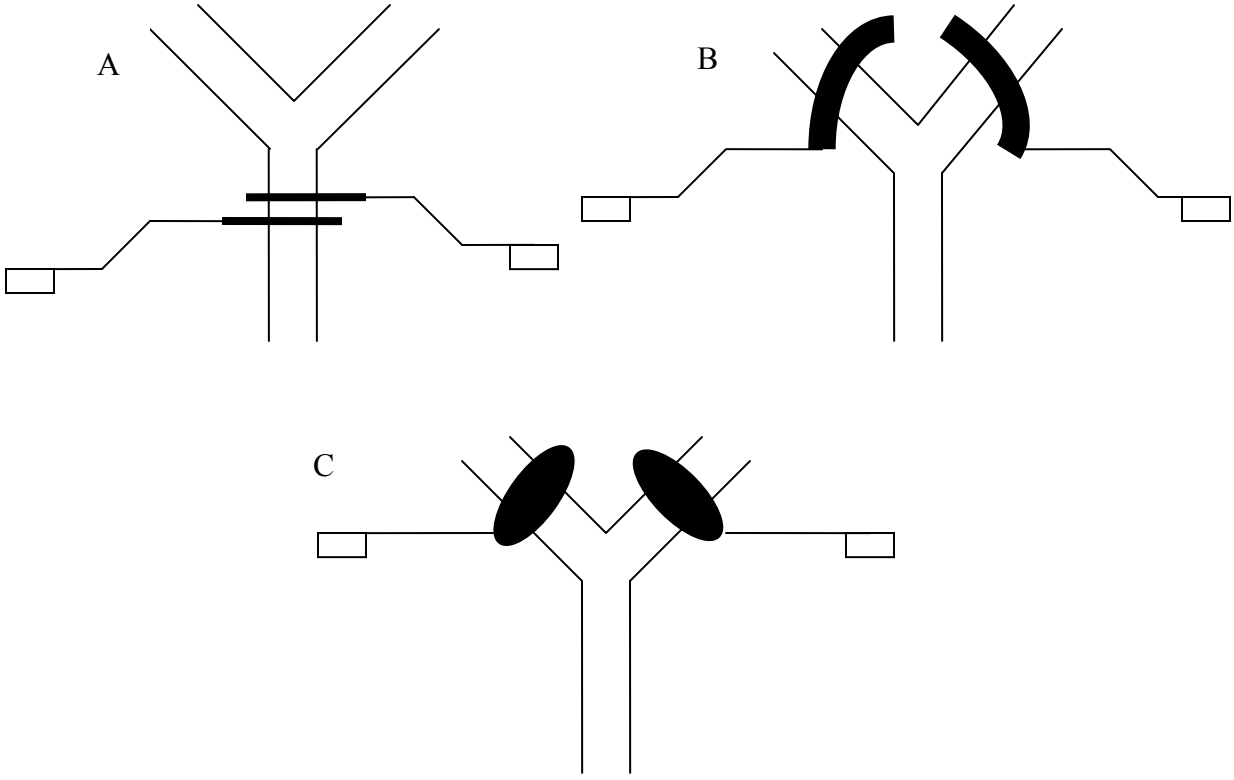

Figure 3-3 Early electrode-fluidic layer designs. Electrodes are depicted in black

3.3.2 Actuation Frequency

The frequency at which the DE was switched from its actuated to its normal state was studied. Frequencies of 10, 20, 30, 40 and 50 Hz were examined and subsequent fluorescence profiles were taken at 1, 3, 5 and 7 mm downstream from the intersection. Again the actuators were energized 180 degrees out of phase with each other. The flow profile that was created at different frequencies stems from the fluids in the two arms being pushed into and out of the mixing channel. Figure 3-4 shows the flow patterns achieved at different frequencies. As can be seen in figure 3-4 the size of the oscillations change with frequency; the higher the frequency the smaller the size of the oscillations. Figure 3-4 also shows the oscillations at different points downstream from the intersection. Moreover, there was a marked difference in flow pattern observed when the potential difference between the electrodes was changed from 1500 V to 2000 V. This change would be expected as can be seen from equation 8 which shows that the change is height of the polymer due to applied electric field is proportional to the square of the electric field.

Another interesting observation was the distance the fluid travel into the other flow stream with varying the frequency. It is evident that as the frequency increased the fluid oscillations, it also resulted in a smaller in volume displaced. This may be due to the fact that as the frequency increases there is not enough time to push all of the fluid into the main mixing channel before the actuator in energized again. This leads to less fluid being "jolted" into the opposite flow stream upon relaxation of the polymer back to its original state. The opposite is true for lower frequencies; the relativity long time in the actuated mode allows enough time for fluid to rush into the additional volume created by the actuation thus a larger volume of fluid is expelled upon relaxation of the polymer. This is evident in Figure 3-3, (also see images in

Appendix A) the periods decrease in size and the distance the oscillations travel into the opposing flow stream also decreases with increasing frequencies.

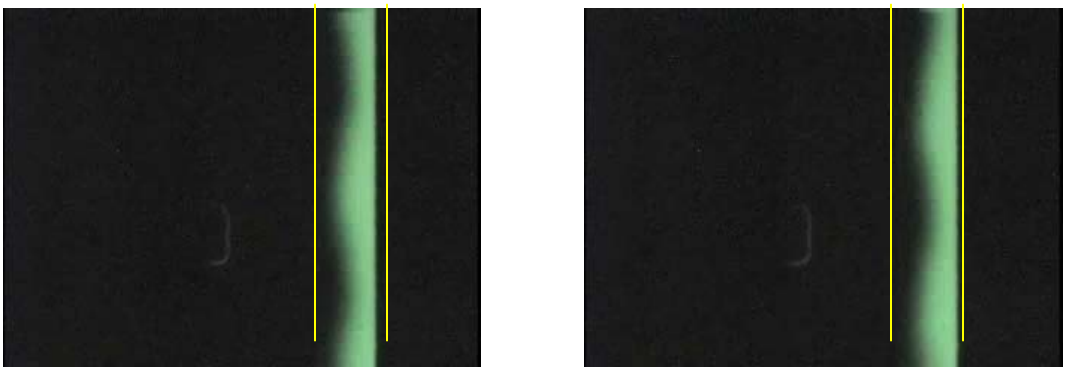

Figure 3-4 Microscope images of channels during different actuation frequency of 10 and 20Hz and electric field differences between electrodes of 1500V at 1mm from intersection. Yellow lines represent channel boundaries

3.3.3 Fluorescence Profiles

Determination of whether complete mixing was occurring with actuation was accomplished by taking fluorescent profiles across the width of the channel at different points downstream from the intersection. A flat profile across the width of the channel is indicative of a complete mixing. Fluorescent profiles at the 1mm, 3mm, 5mm and 7mm downstream at 10-50Hz actuation frequency were all taken, figure 3-5. To briefly describe data collection, average intensity profiles were taken by averaging over the distance of one oscillation that was previously described and shown in figure 3-4. This method was chosen as a means of determining the average extent of mixing because mixing is incomplete.

Figure 3-5 Image of oscillation produced upon actuation. The area in the boxed region shows example of distance over which the average fluorescence profile was taken.

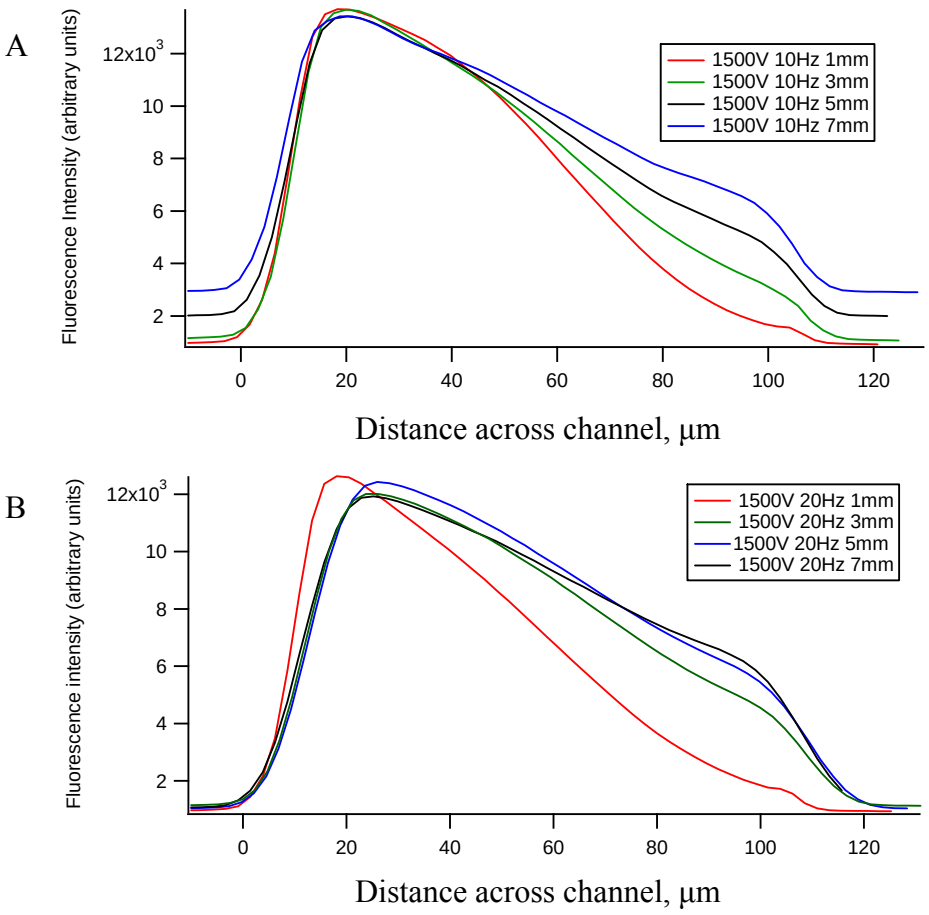

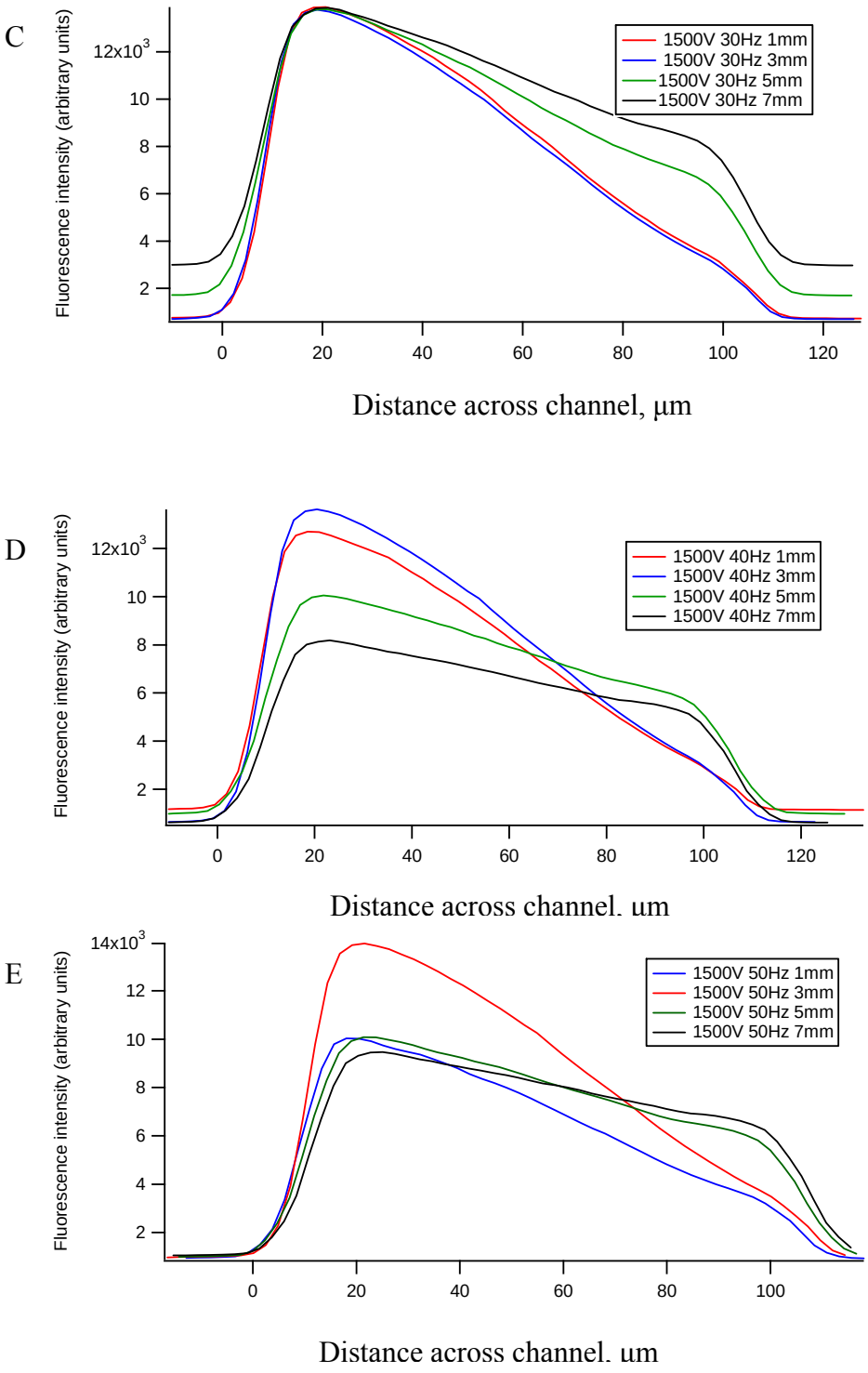

Figure 3-6 Average fluorescence profile at 1, 3, 5 and 7mm downstream from intersection for 1500V difference between electrodes for 10, 20, 30, 40 and 50Hz actuation frequencies.

F

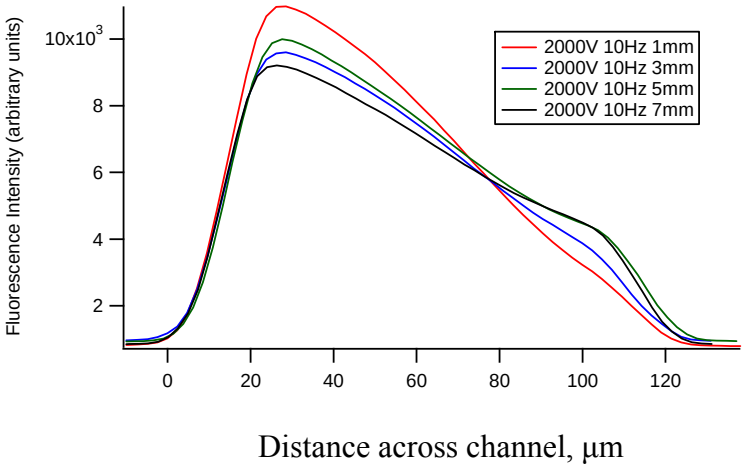

Distance across channel, µm

G

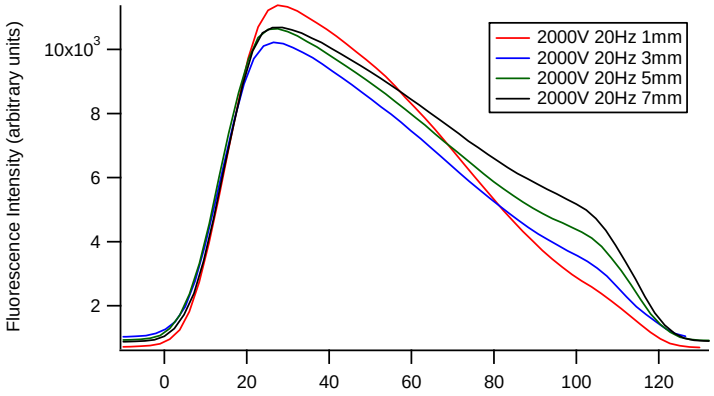

Distance across channel, µm

H

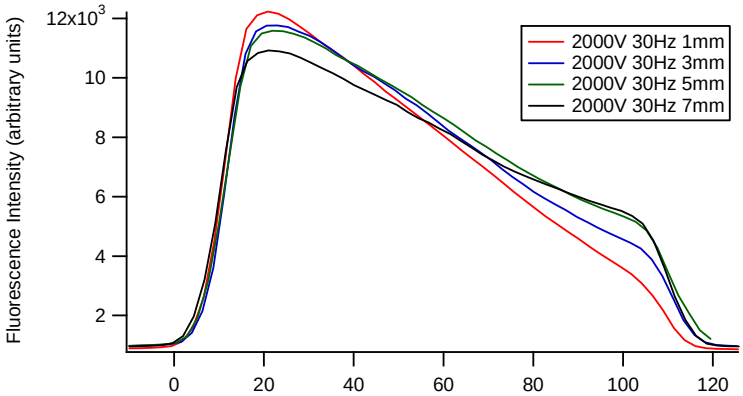

Distance across channel, µm

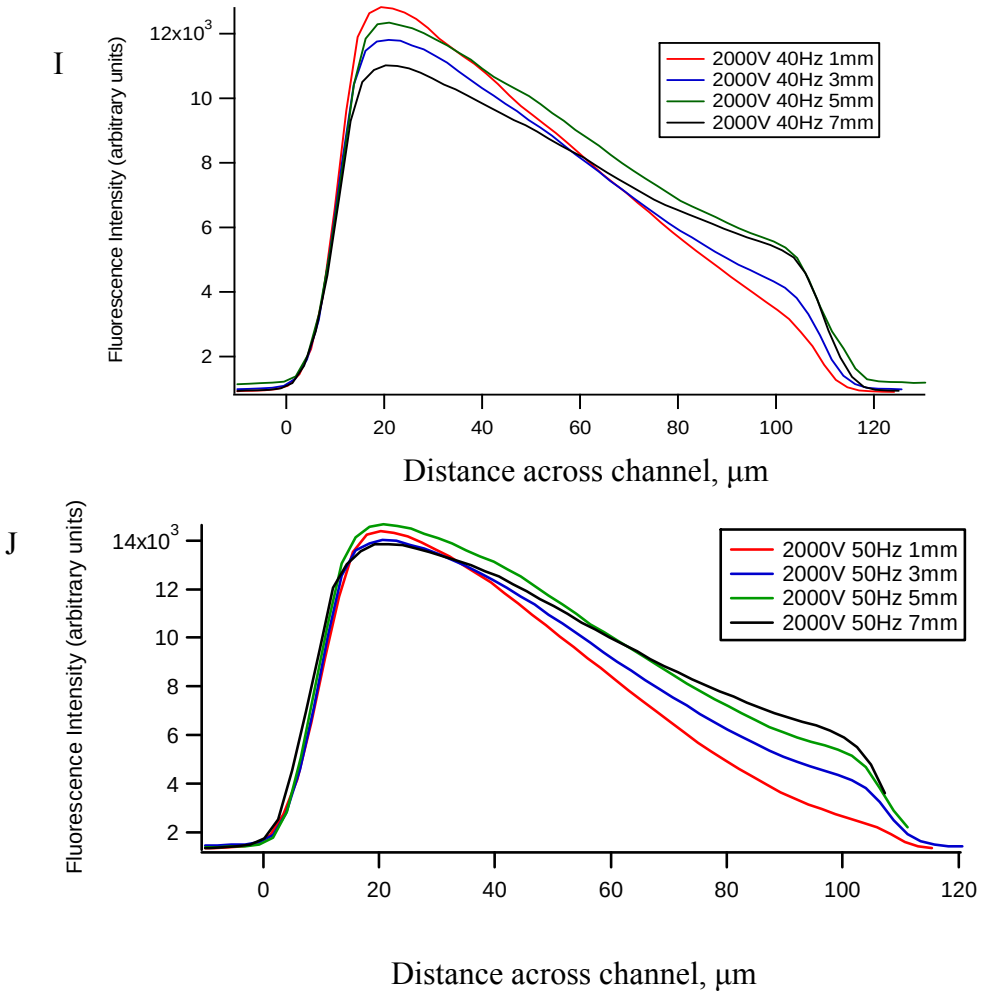

Figure 3-7 Average fluorescence profile at 1, 3, 5 and 7mm downstream from intersection for 2000V difference between electrodes for actuation frequencies 10, 20, 30, 40 and 50Hz actuation frequency.

From figure 3-6 and 3-7, a few conclusions can be drawn. The fluorescence profiles' average intensity decreases as distance downstream increases. This could be evidence of dilution due to mixing. Furthermore, the slope of the plots decreases with distance downstream. A slope of zero is expected for complete mixing (flat fluorescent profile) therefore a decreasing slope shows progress towards complete mixing. From the data, a flat profile would not be obtained until

beyond the outlet of the mixing channel. The mixing channel is 2cm so mixing based on diffusion at 500V/cm would need longer than 2cm to reach 100%.

To quantitatively express the extent of mixing, the following equation was used:

Equation 11

$$MixingIndex = \frac{\sigma}{average}$$

where σ is the standard deviation of the fluorescence profile and the average is average fluorescence intensity over one oscillation. Using this equation a mixing index of 1%, for example, is indicative of 99% mixing. A comparison of the mixing indices of 1500V and 2000V differences between the electrodes at different frequencies was performed. Figure 3-6 shows the mixing indices of 1500V and 2000V at an actuation frequency of 10-50Hz. The plot for 2000V and 10Hz shows a continuous decrease in mixing index with distance while the 1500V 10Hz only shows a significant drop in mixing index beginning at 5mm downstream. A comparison at 7mm shows that the 1500V at 10Hz plot reaches a mixing index of about 0.35 (65% mixing) while the 2000V at 10Hz plot has a mixing index of about 0.45 (55%) mixing. From all of the mixing indices plots, the 1500V difference between the electrodes seems to perform better by 7mm compared to the 2000V difference between electrodes. .

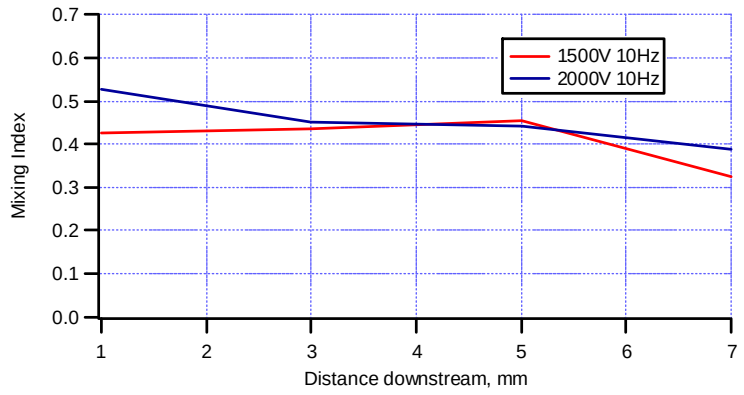

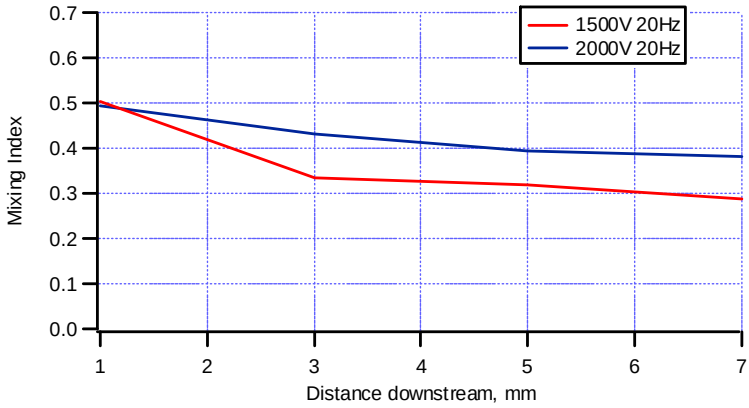

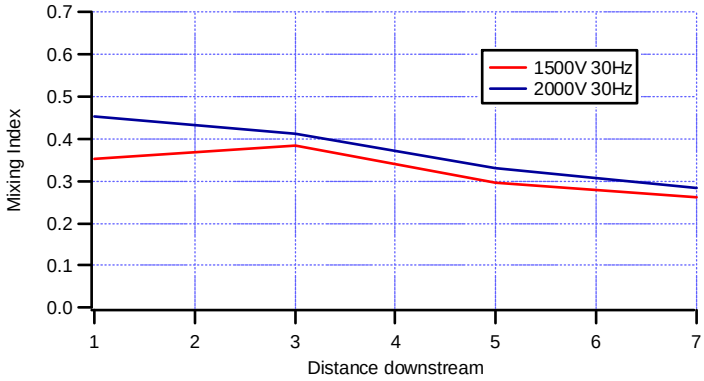

Figure 3-8 Mixing Indicies of 1500V and 2000V difference in electrode potential at 10, 20 and 30Hz frequencies of actuation.

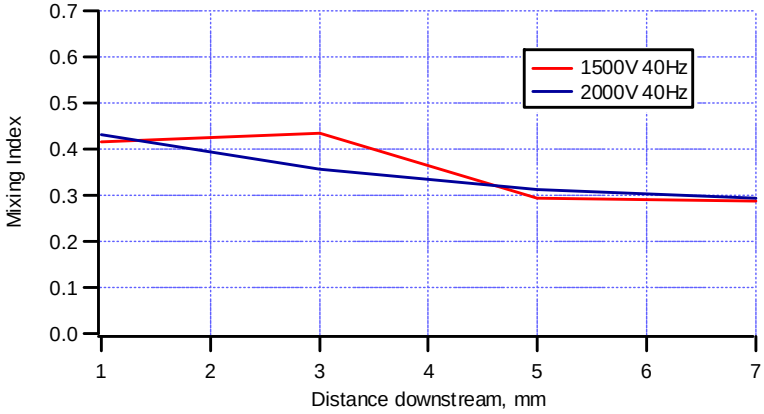

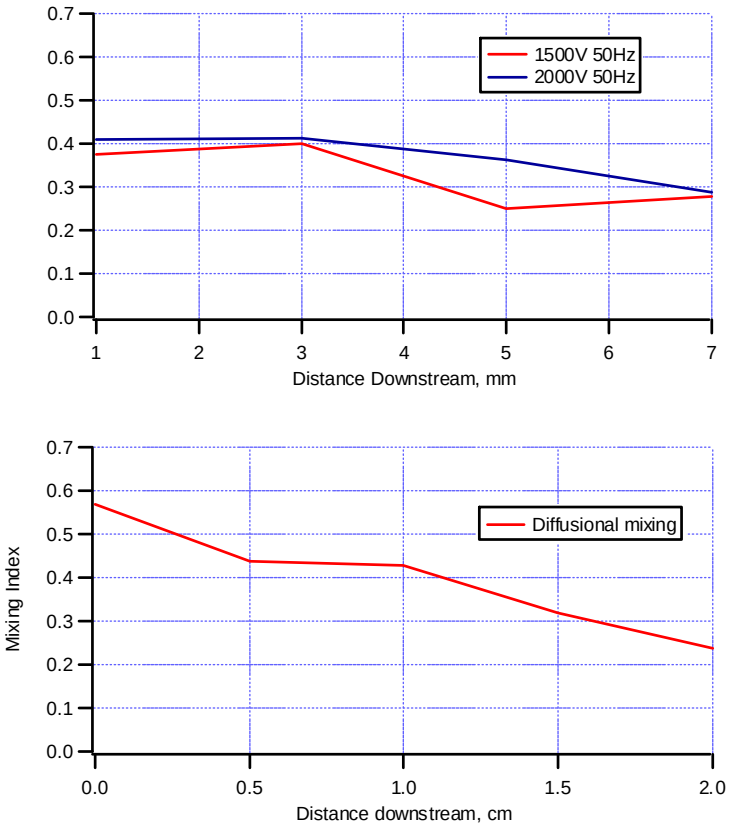

Figure 3-9 Mixing Indices of 1500V and 2000V electrode difference for actuation frequency of 40 and 50Hz and diffusional based mixing.

3.4 Conclusions and Future Directions

In conclusion, this method of mixing shows great promise as a means to achieve fast and efficient mixing. For 1500V and 2000v differences between electrodes, 72% percent mixing was achieved within 7mm on our device. Moreover, this device is easily fabricated from well developed lithography techniques. Furthermore, fluorescent microscope images were taken to show the oscillations produced in the fluid flow upon changing the frequency of actuation. Despite all of the promise exhibited by this device, there are a few areas that need to be explored to tap into the full potential of this device for performing efficient and fast mixing.

One area that should be explored to optimize this mixing technique is to use hydrodynamic flow instead of electrokinetically driving the fluid streams. This issue may

improve the mixing process because of the fluid velocity control that would come with driving the fluids using a dual syringe pump. This would also allow for more time for diffusion to take place since the fluid would be driven at a slower pace. From a materials perspective, there would be less heat generated from the electric field in the channel thus reducing the chance of PDMS breakdown due to heat production. Furthermore, the goal of this device is to perform passive mixing therefore increasing the interface of two flow streams is paramount. We have exhibited that the oscillations produced can achieve this by decreasing the size of the fluid oscillations produced during actuation. The smaller the oscillations the greater the interface would be, therefore higher frequencies should be the focus of this project down the line. Since we were limited by technology such as the LabView program's limits on applied frequency, the camera's image collecting capability the method that will be pursued to optimize this device is to modify channel dimensions. A change is channel dimensions would improve mixing by increasing the Reynolds number. Since the Reynolds number is proportionate to the characteristic channel dimension, an increase in width or depth would result in an increase in the Reynolds number. This could be easily accomplished by designing a different mask in the case of channel width or using a photoresist such as SU-8 2035 to etch deeper channels. Lastly, using different, softer elastomers would be beneficial because softer polymers would have lower Young's moduli, thus resulting in higher Δh values. Higher Δh values would in turn result in higher amounts of fluid displaced during actuation and relaxation. Moreover, polymers with higher dielectric constants should be examined since the amount of strain produced is directly proportionate to the dielectric constant.

We believe that exploring the aforementioned areas would lead to a device that produces fast and efficient mixing for implementation onto microchips. The advantages and ease of

implementation of the requirements necessary for this mixing technique lead to a device that incorporates mixing very easily.

Appendix A - Additional images

Fluorescence Images of flow created by different actuation frequencies

Figure A-1 Fluorescent image of flow generated by out-of-phase actuation for 1500V, 10Hz and 1mm downstream. Left image shows buffer stream actuation and right image shows fluorescein reservoir actuation

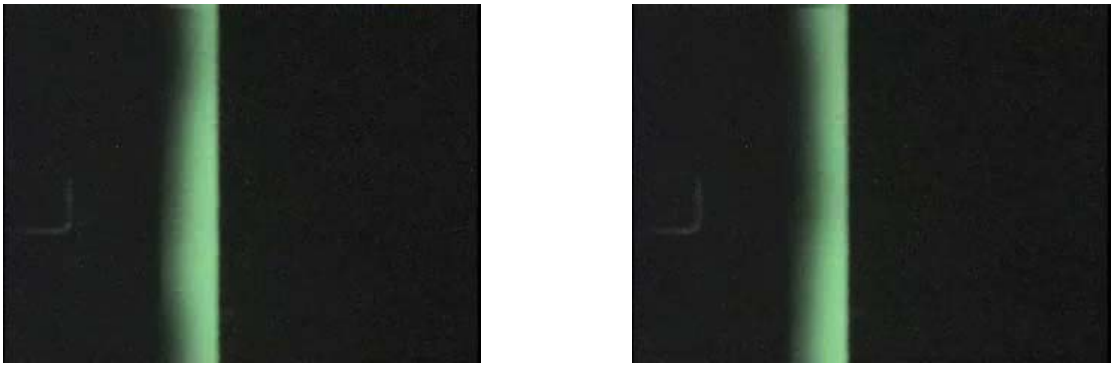

Figure A-2 Fluorescent image of flow generated by out- of-phase actuation for 1500V, 10Hz, and 3mm downstream. Left image shows buffer stream actuation and right image shows fluorescein reservoir actuation.

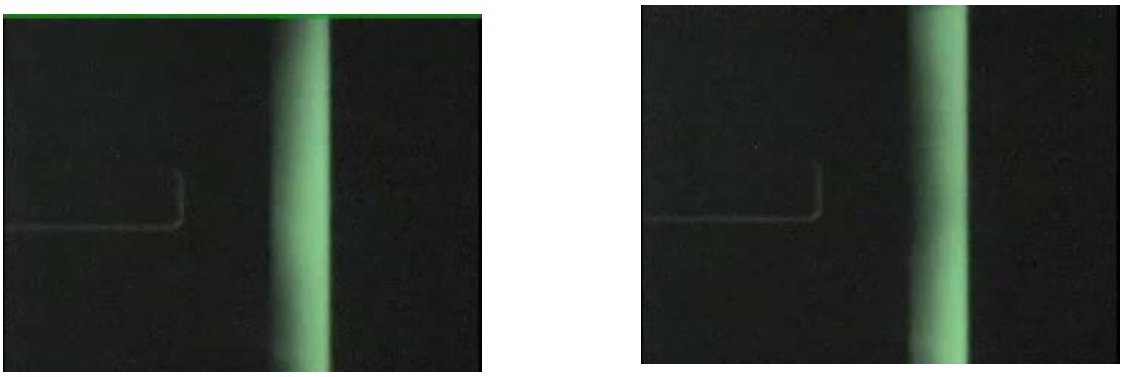

Figure A-3 Fluorescent image of flow generated by out- of-phase actuation for 1500V, 10Hz, and 5mm downstream. Left image shows buffer stream actuation and right image shows fluorescein reservoir actuation.

Figure A-4 Fluorescent image of flow generated by out- of-phase actuation for 1500V, 10Hz, and 5mm downstream. Left image shows buffer stream actuation and right image shows fluorescein reservoir actuation.

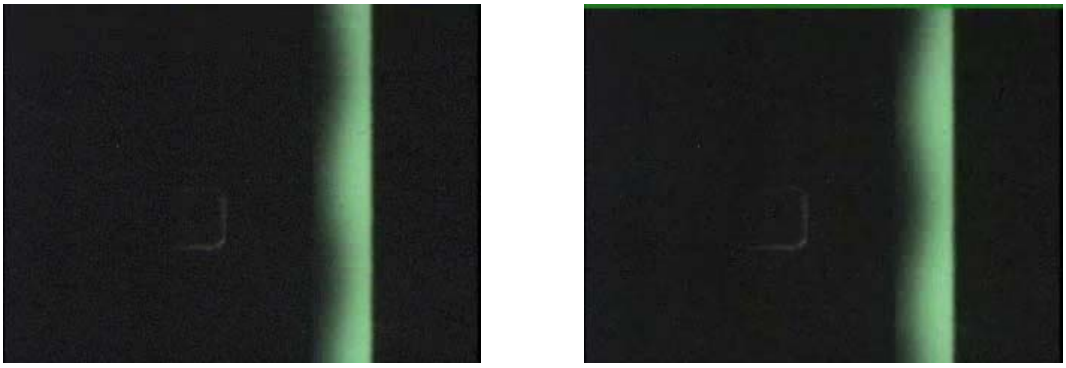

Figure A-5 Fluorescent image of flow generated by out- of-phase actuation for 1500V, 20Hz, and 3mm downstream. Left image shows buffer stream actuation and right image shows fluorescein reservoir actuation.

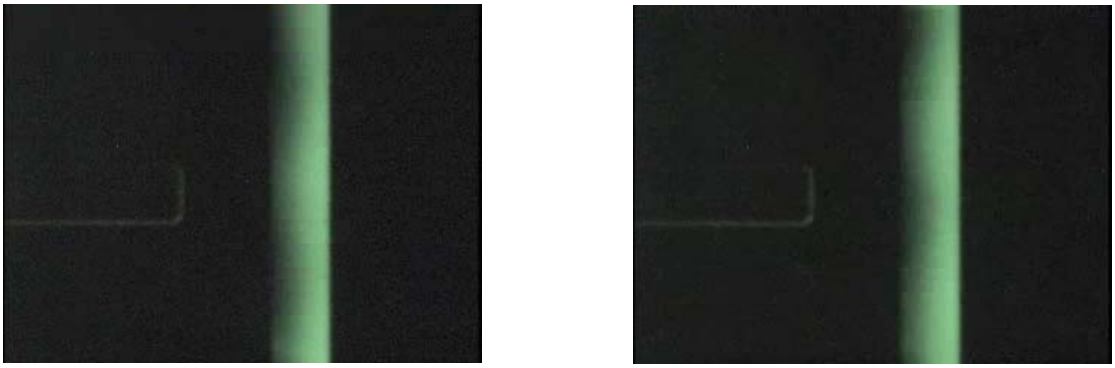

Figure A-6 Fluorescent image of flow generated by out- of-phase actuation for 1500V, 20Hz, and 5mm downstream. Left image shows buffer stream actuation and right image shows fluorescein reservoir actuation.

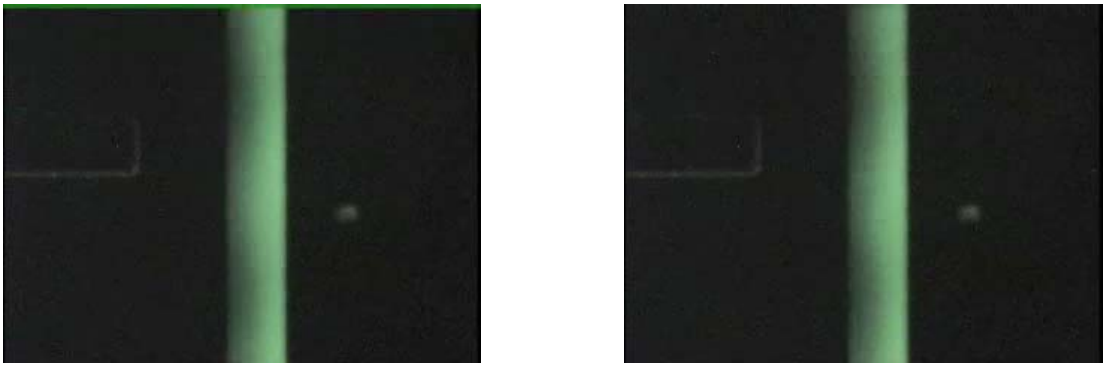

Figure A-7 Fluorescent image of flow generated by out- of-phase actuation for 1500V, 20Hz, and 7mm downstream. Left image shows buffer stream actuation and right image shows fluorescein reservoir actuation.

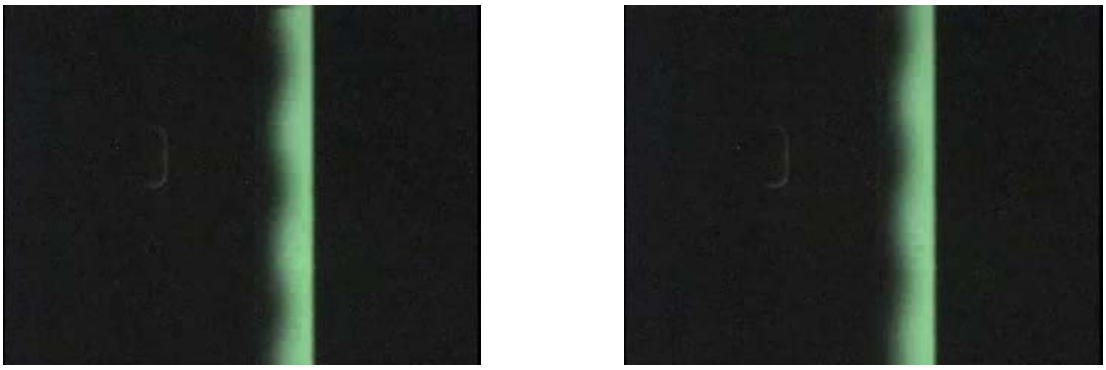

Figure A-8 Fluorescent image of flow generated by out- of-phase actuation for 1500V, 30Hz, and 1mm downstream. Left image shows buffer stream actuation and right image shows fluorescein reservoir actuation.

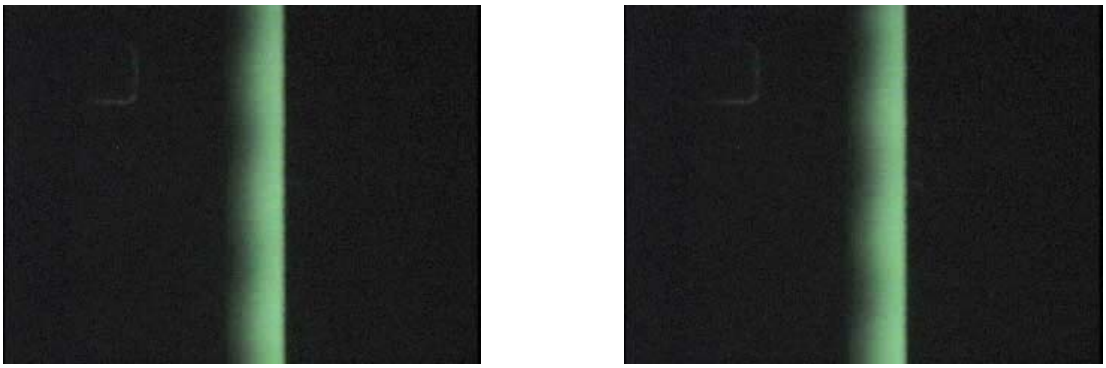

Figure A-9 Fluorescent image of flow generated by out- of-phase actuation for 1500V, 30Hz, and 3mm downstream. Left image shows buffer stream actuation and right image shows fluorescein reservoir actuation.

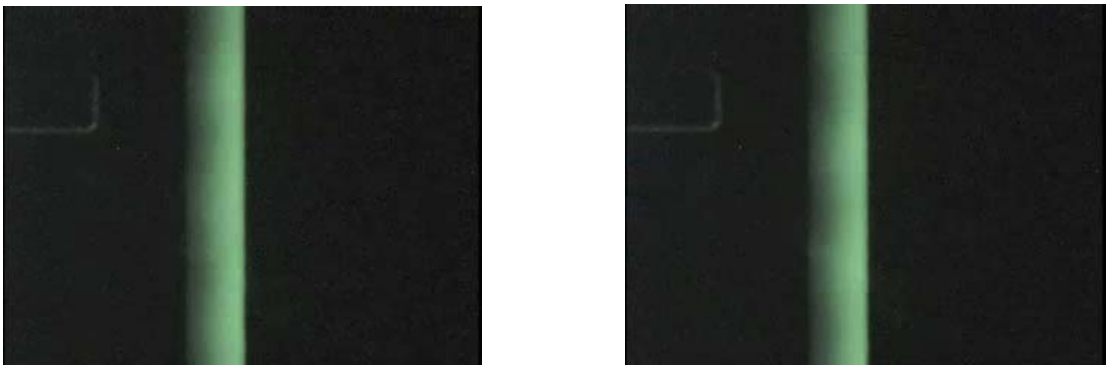

Figure A-10 Fluorescent image of flow generated by out- of-phase actuation for 1500V, 30Hz, and 5mm downstream. Left image shows buffer stream actuation and right image shows fluorescein reservoir actuation.

Figure A-11 Fluorescent image of flow generated by out- of-phase actuation for 1500V, 30Hz, and 7mm downstream. Left image shows buffer stream actuation and right image shows fluorescein reservoir actuation.

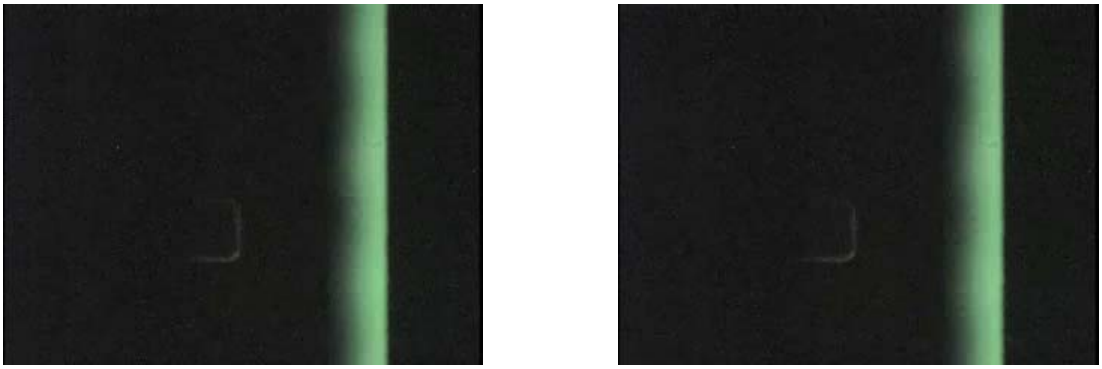

Figure A-12 Fluorescent image of flow generated by out- of-phase actuation for 1500V, 40Hz, and 3mm downstream. Left image shows buffer stream actuation and right image shows fluorescein reservoir actuation.

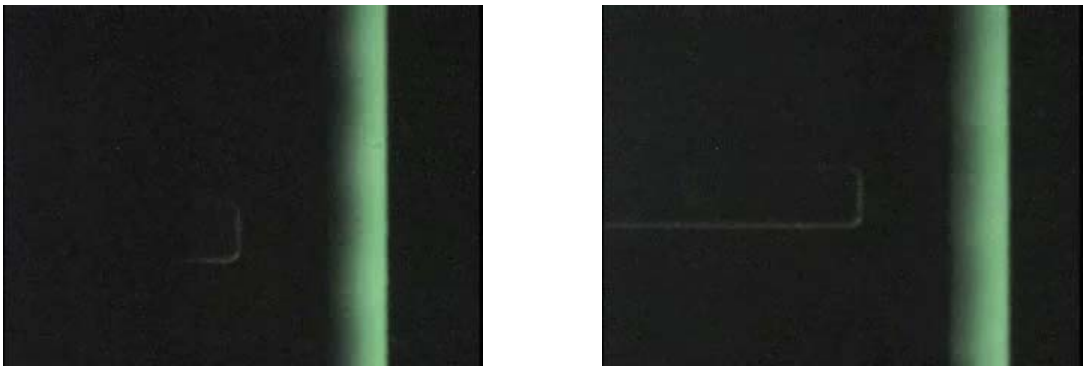

Figure A-13 Fluorescent image of flow generated by out- of-phase actuation for 1500V, 40Hz, and 5mm downstream. Left image shows buffer stream actuation and right image shows fluorescein reservoir actuation.

Figure A-14 Fluorescent image of flow generated by out- of-phase actuation for 1500V, 40Hz, and 7mm downstream. Left image shows buffer stream actuation and right image shows fluorescein reservoir actuation.

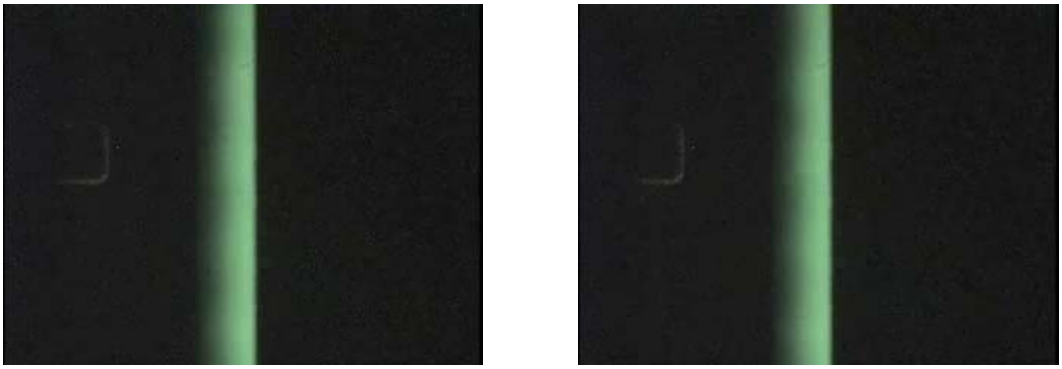

Figure A-15 Fluorescent image of flow generated by out- of-phase actuation for 1500V, 50Hz, and 3mm downstream. Left image shows buffer stream actuation and right image shows fluorescein reservoir actuation.

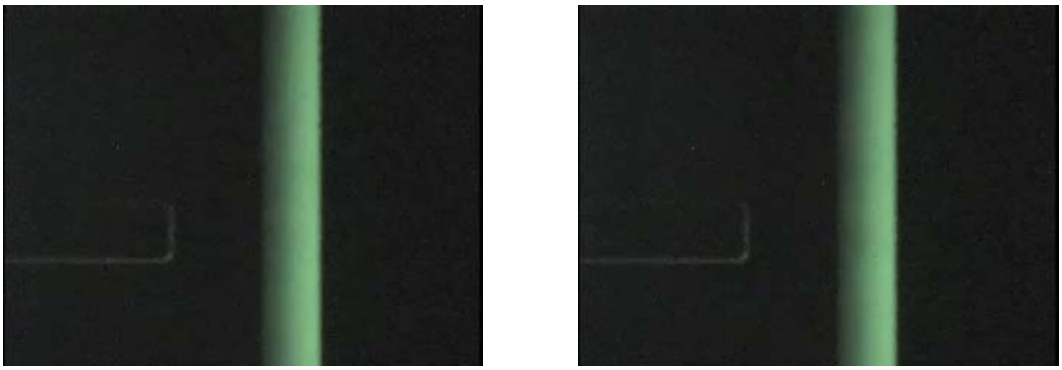

Figure A-16 Fluorescent image of flow generated by out- of-phase actuation for 1500V, 50Hz, and 5mm downstream. Left image shows buffer stream actuation and right image shows fluorescein reservoir actuation.

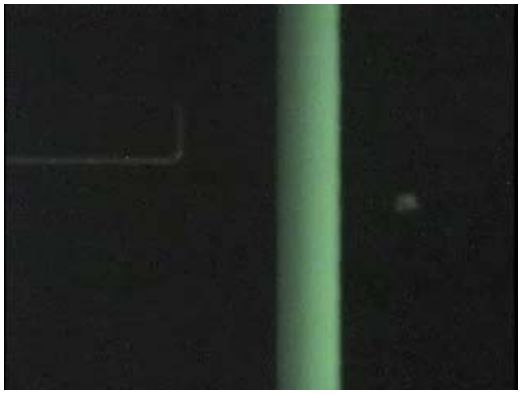

Figure A-17 Fluorescent image of flow generated by out- of-phase actuation for 1500V, 50Hz, and 7mm downstream.

Figure A-18 Fluorescent image of flow generated by out- of-phase actuation for 2000V, 20Hz, and 3mm downstream. Left image shows buffer stream actuation and right image shows fluorescein reservoir actuation.

Figure A-19 Fluorescent image of flow generated by out- of-phase actuation for 2000V, 20Hz, and 5mm downstream. Left image shows buffer stream actuation and right image shows fluorescein reservoir actuation.

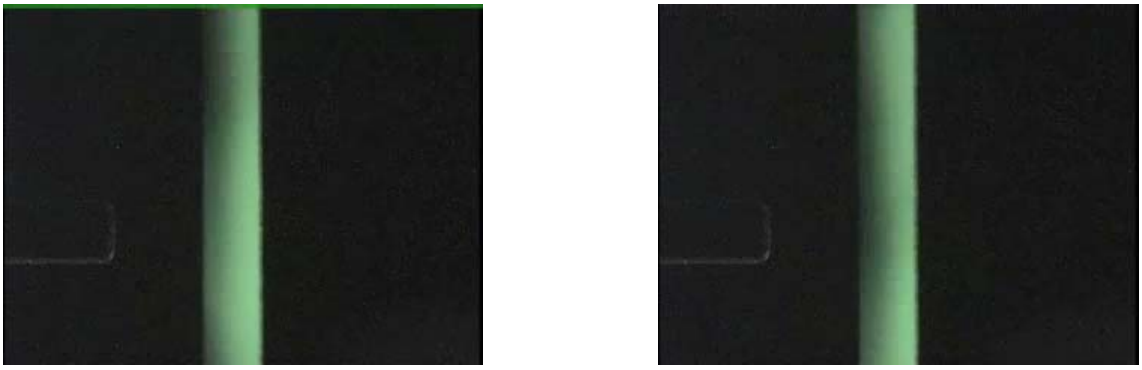

Figure A-20 Fluorescent image of flow generated by out- of-phase actuation for 2000V, 20Hz, and 7mm downstream. Left image shows buffer stream actuation and right image shows fluorescein reservoir actuation.

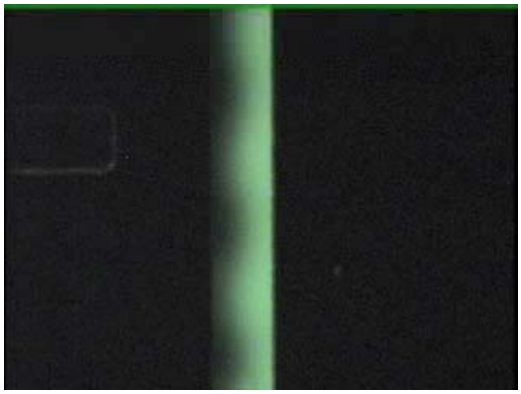

Figure A-21 Fluorescent image of flow generated by out- of-phase actuation for 2000V, 30Hz, and 3mm downstream.

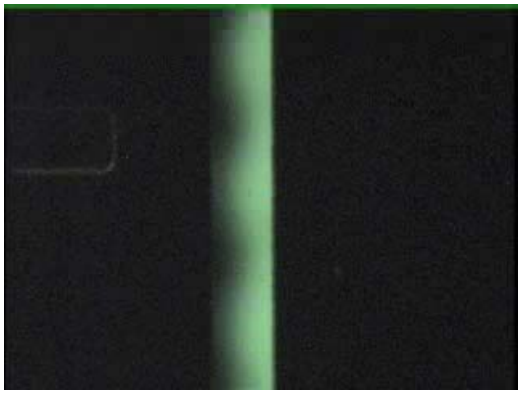

Figure A-22 Fluorescent image of flow generated by out- of-phase actuation for 2000V, 30Hz, and 5mm downstream.

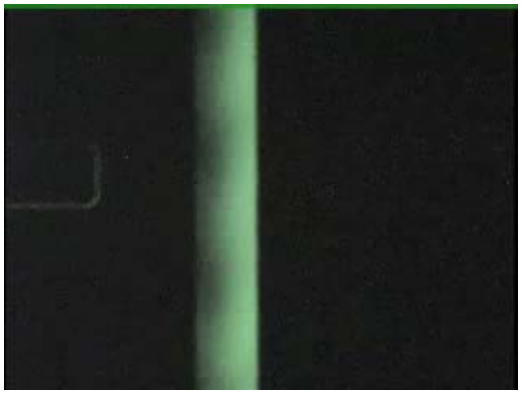

Figure A-23 Fluorescent image of flow generated by out- of-phase actuation for 2000V, 30Hz, and 7mm downstream.

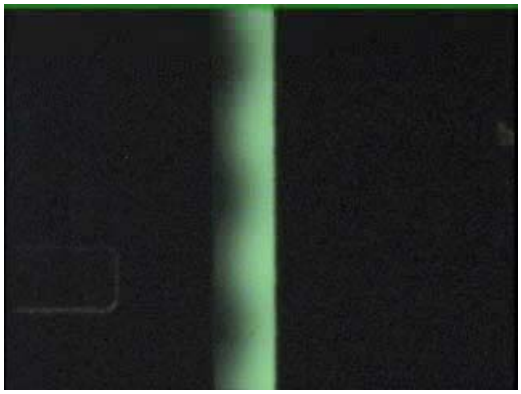

Figure A-24 Fluorescent image of flow generated by out- of-phase actuation for 2000V, 40Hz, and 3mm downstream.

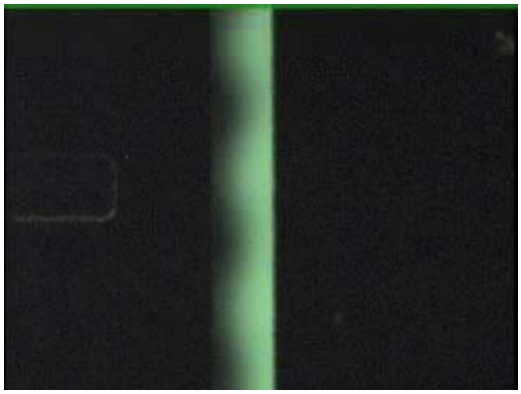

Figure A-25 Fluorescent image of flow generated by out- of-phase actuation for 2000V, 40Hz, and 5mm downstream.

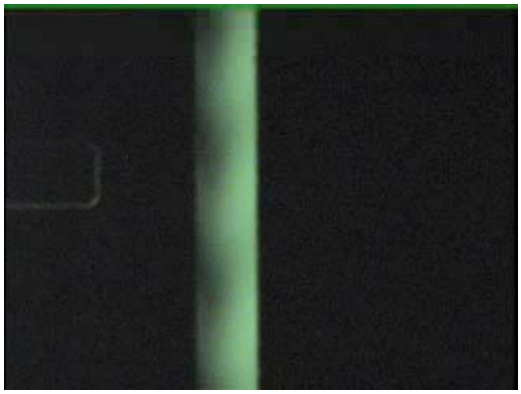

Figure A-26 Fluorescent image of flow generated by out- of-phase actuation for 2000V, 40Hz, and 7mm downstream.

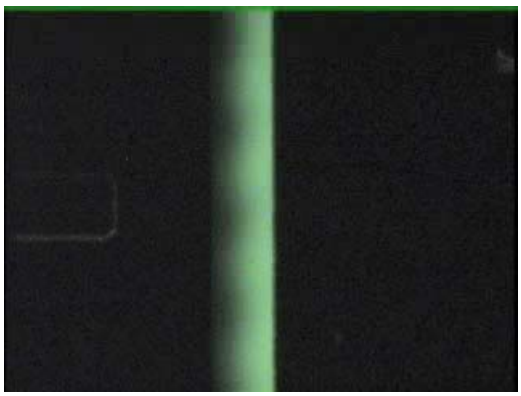

Figure A-27 Fluorescent image of flow generated by out- of-phase actuation for 2000V, 50Hz, and 3mm downstream.

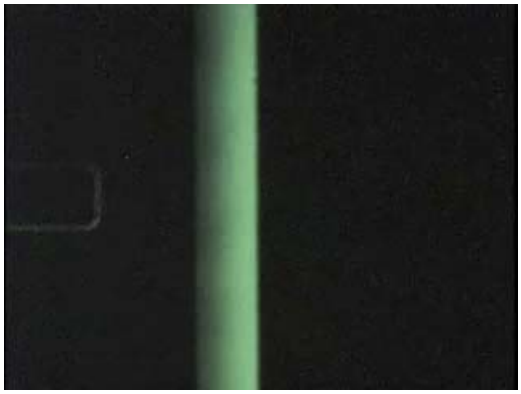

Figure A-28 Fluorescent image of flow generated by out- of-phase actuation for 2000V, 50Hz, and 5mm downstream.

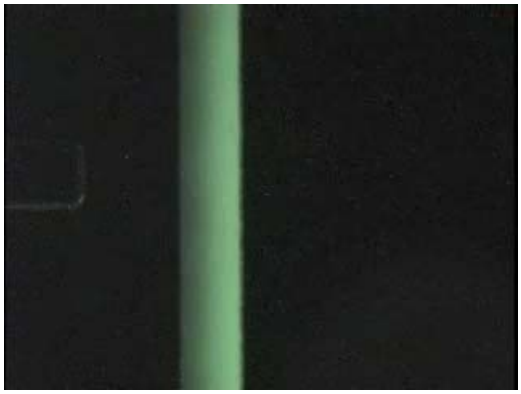

Figure A-29 Fluorescent image of flow generated by out- of-phase actuation for 2000V, 50Hz, and 7mm downstream.

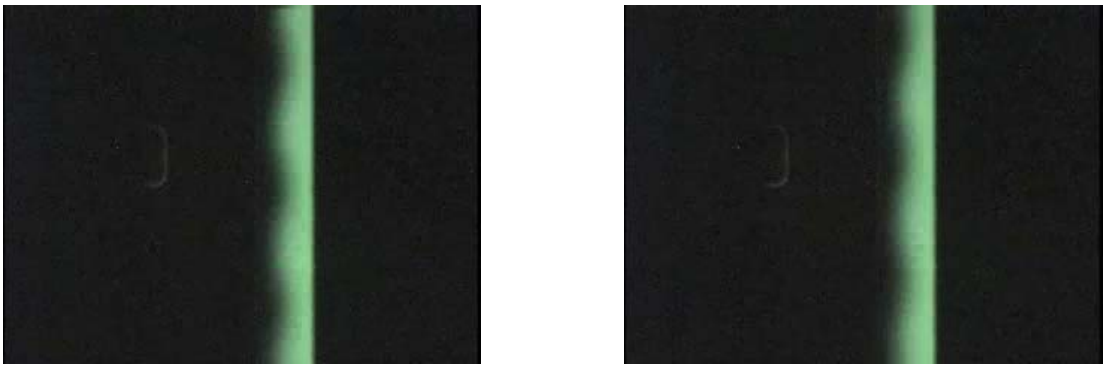

Figure A-30 Fluorescent image of flow generated by out- of-phase actuation for 1500V, 30Hz, and 1mm downstream. Left image shows buffer stream actuation and right image shows fluorescein reservoir actuation.

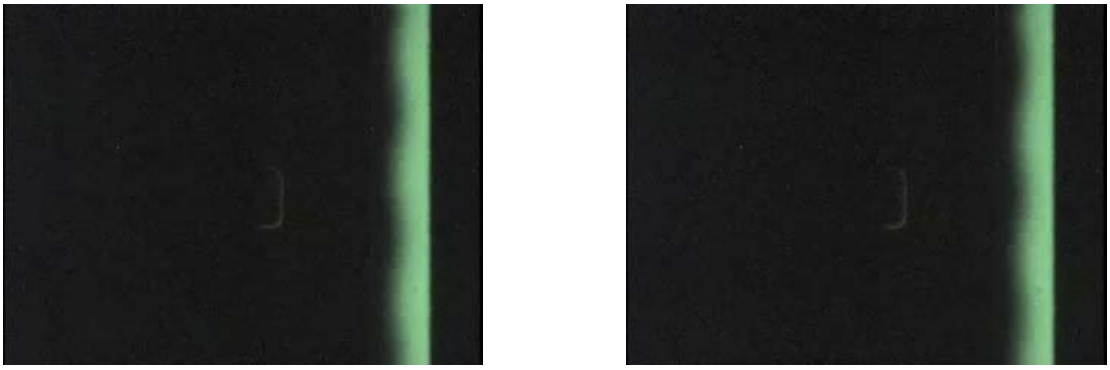

Figure A-31 Fluorescent image of flow generated by out- of-phase actuation for 1500V, 40Hz, and 1mm downstream. Left image shows buffer stream actuation and right image shows fluorescein reservoir actuation.

Figure A-32 Fluorescent image of flow generated by out- of-phase actuation for 1500V, 50Hz, and 1mm downstream. Left image shows buffer stream actuation and right image shows fluorescein reservoir actuation.

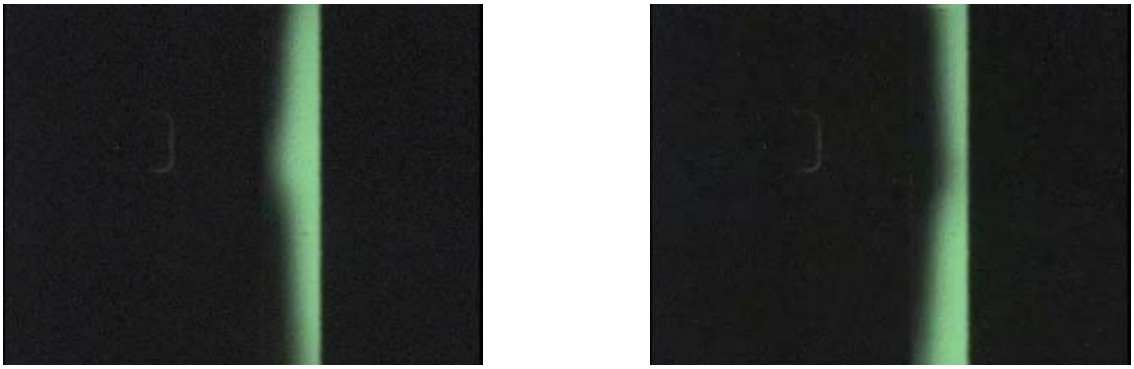

Figure A-33 Fluorescent image of flow generated by out- of-phase actuation for 2000V, 10Hz, and 1mm downstream. Left image shows buffer stream actuation and right image shows fluorescein reservoir actuation.

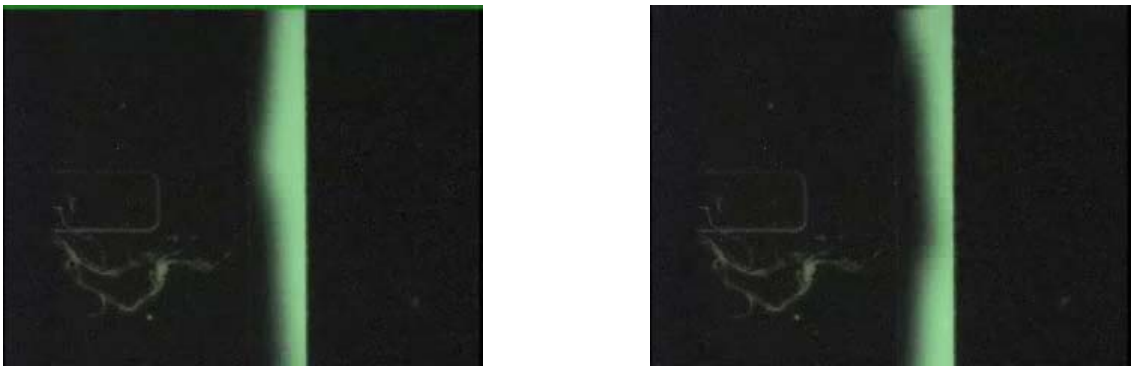

Figure A-34 Fluorescent image of flow generated by out- of-phase actuation for 2000V, 20Hz, and 1mm downstream. Left image shows buffer stream actuation and right image shows fluorescein reservoir actuation.

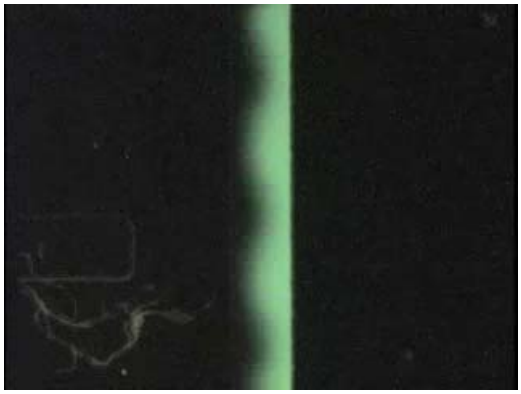

Figure A-35 Fluorescent image of flow generated by out- of-phase actuation for 2000V, 30Hz, and 1mm downstream. Left image shows buffer stream actuation and right image shows fluorescein reservoir actuation.

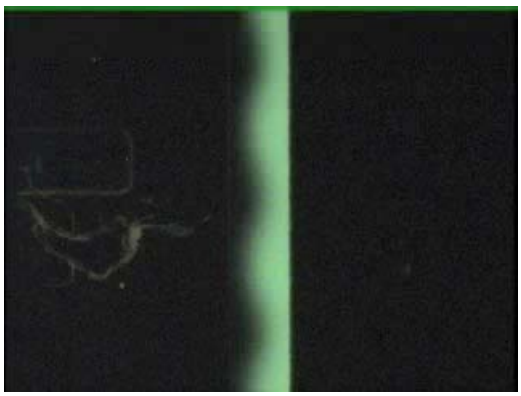

Figure A-36 Fluorescent image of flow generated by out- of-phase actuation for 2000V, 40Hz, and 1mm downstream. Left image shows buffer stream actuation and right image shows fluorescein reservoir actuation.